Biomass and Bioenergy 210 (2026) 109151

Contents lists available at ScienceDirect

Biomass and Bioenergy

journal homepage: www.elsevier.com/locate/biombioe

Effect of physicochemical properties of fossil and biogenic carbons on short-term performances of molten hydroxide direct carbon fuel cell

Sara Scolari *, Davide Mombelli, Gianluca Dall'Osto, Carlo Mapelli

Politecnico di Milano, Dipartimento di Meccanica, Via Privata Giuseppe La Masa 1, 20156, Milano, Italy

ARTICLE INFO

Keywords:
Molten hydroxide-direct carbon fuel cell
biochar
Chemical characterization
Electrochemical characterization

ABSTRACT

The transition toward low-emission energy systems requires alternative conversion technologies capable of valorizing carbon-rich waste streams. Molten hydroxide direct carbon fuel cells (MH-DCFCs) offer a promising route for efficient energy production from solid biogenic fuels at temperatures below 600 °C. However, a systematic understanding of how the physicochemical properties of carbon-rich materials affect the short-term cell performance is necessary. In this work a total of 9 fuels, of which 7 of biogenic origin and 2 of fossil origin, were used. Each fuel was comprehensively investigated by means of morphological, mineralogical, and chemical characterization, further to particle analysis, proximate analysis, and wettability assessment. The electrochemical efficiency of the MH-DCFC for each matrix was evaluated by open-circuit voltage (OCV) and linear sweep voltammetry (LSV) at 450 °C. Results demonstrated that fuel reactivity and performance arise from complex interactions between volatile matter (VM), fixed carbon (FC), ash content, and particle morphology. Optimal OCV and power output (maximum value reached 1060 mV and 6.22 mW cm^{-2}) corresponded to fuels with a FC/VM ratio from 1 to 2, moderate ash content (<30 wt%), and elongated, porous particles (aspect ratio of about 0.5 and 33% porosity). Impurities such as KCl and iron oxides further promote electrochemical activity, while SiO_2 inhibit it. Comparison with literature data confirms the observed trends and validates the proposed correlations.

1. Introduction

In recent years, European Union (EU) stands out for its efforts in producing clean and renewable energy. In 2024, renewables covered 47% of EU electricity, while fossil share declined to 29% [1]. Although solar remained the fastest growing power source, and wind the second largest above gas and below nuclear, wind and solar energy greatly depend on weather variability [1]. For this reason, the need to find flexible, storable and low-emission energy sources is still one of the main topics to address electricity transition to 2030.

Fuel cells are recently considered as one of the most promising technologies for the decarbonization of the energy sector, owing to their high efficiency, modularity, and potential compatibility with renewable and waste-derived fuels [2].

Among the different fuel cell technologies, solid oxide fuel cells (SOFCs) have attracted considerable attention due to their fuel flexibility and their ability to operate with carbon-containing fuels. Many works have explored the conversion of biomass-derived syngas into electricity using SOFCs [3–6]. However, this technology still faces critical challenges. Anodes suffer the sulfur contained in the syngas, which is one of the main causes of degradation of cell performance, and the anode could be also damaged due to carbon deposition and following decomposition [3]. These limitations lead to an increased interest in alternative configurations capable of directly exploiting solid carbonaceous fuels.

Direct carbon fuel cells (DCFCs) represent a particularly attractive option, as they allow the direct electrochemical oxidation of solid carbon at the anode. DCFCs could theoretically achieve conversion efficiencies up to 80%, approximately double those of conventional coal-fired power plants, while also enabling near-complete fuel utilization [7,8]. Most of the studies on solid oxide direct carbon fuel cells (SO-DCFCs) have focused on fossil-derived fuels [9–13], obtaining different power density according to the material (e.g., 53.4 and 51.3 mW cm^{-2} with anthracite and lignite, respectively [10,14] mW cm^{-2} with petroleum coke [9] and graphite [11], respectively). More recently, increasing attention has been devoted to bio-wastes [15–17], like lignite producing 62.7 mW cm^{-2} [10], and bio-based carbon fuels, like charcoal obtaining 105 mW cm^{-2} [18].

* Corresponding author.
E-mail address: Sara.scolari@polimi.it (S. Scolari).

https://doi.org/10.1016/j.biombioe.2026.109151
Received 16 January 2026; Received in revised form 18 February 2026; Accepted 18 February 2026
Available online 20 February 2026
0961-9534/© 2026 The Authors. Published by Elsevier Ltd. This is an open access article under the CC BY license (http://creativecommons.org/licenses/by/4.0/).

Beyond their renewable nature and their potential role in waste management, the use of biochar in DCFCs offers additional systemic advantages. In particular, the electrochemical oxidation of solid carbon produces a CO_2-rich exhaust stream, which is intrinsically simpler to capture than flue gases containing a complex mixture of other pollutants [8]. Despite these advantages, SO-DCFCs are typically operated at high temperatures, between 800 and 1000 °C [8]. This represents a major barrier in terms of material durability, system complexity, and energy consumption. Under such conditions, cell heating generally relies on direct electrical input, limiting the overall sustainability of the process. Lowering the operating temperature would significantly expand the range of viable thermal management strategies, including the integration of industrial waste heat streams or the use of low-grade heat sources.

In this context, molten hydroxide direct carbon fuel cells (MH-DCFCs) emerge as a promising alternative. Thanks to the use of molten hydroxide electrolytes (typically KOH/NaOH mixtures), MH-DCFCs can operate at temperatures below 600 °C while providing more than acceptable electric performance [8]. These operating conditions make MH-DCFCs particularly suitable for synergistic integration with industrial processes characterized by the availability of medium- and low-temperature waste heat. For example, waste heat streams are commonly available in steelmaking processes, including blast furnace (BF) and direct reduced iron (DRI) top gases (400-450 °C) [19,20], as well as electric arc furnace (EAF) off-gases, which are often cooled from higher temperatures to protect downstream dust-abatement systems [21]. Rather than being dissipated, this thermal energy could be valorised to supply the heat required for low-temperature MH-DCFC operation, contributing to the overall efficiency and sustainability of the industrial process [22].

Several studies have already demonstrated the feasibility of operating MH-DCFCs with a wide range of carbonaceous fuels, including fossil-based materials (different electrolyte mixtures caused a variation in power density from 37 to 170 mW cm^{-2} [23]), like coal (36.8 mW cm^{-2}) [24] and coke (49.6 mW cm^{-2}) [25], and biochars (32.8 mW cm^{-2}) [24,26], like olive pomace (10 mW cm^{-2}) [27] and sewage sludge (23.5 mW cm^{-2}) [25]. However, despite the growing number of tested fuels, a fundamental scientific gap remains.

The authors identified a lack of a systematic and comprehensive correlation between the physicochemical properties of carbon-based fuels and their electrochemical performance in MH-DCFCs, which represents a significant limitation in the field. The most extensive comparative study is that of Kacprzak et al. [24], who investigated nine different fossil and bio-based carbon materials. While this work provides a valuable experimental dataset, the analysis primarily focuses on comparisons between fuels of similar nature and does not establish global correlations linking fuel properties to cell performance across the entire dataset. As a result, general trends and key physicochemical features affecting optimal MH-DCFC performance cannot be clearly identified. Partial correlations have been proposed in other studies; for instance, Kaklidis et al. [28] observed an increase in power density with increasing volatile matter content. Nevertheless, deeper and more systematic relationships involving additional parameters, such as fixed carbon, ash content and composition, and morphological characteristics, are still missing.

The aim of this work is to address this gap by systematically investigating the impact of the physicochemical properties of fuel on the electrochemical performance of a low-temperature short-term MH-DCFC. Nine different carbon-rich fuels were evaluated, of which only two are of fossil origin (anthracite and coke), while the remaining materials are derived from biomass or waste streams. Each fuel was comprehensively characterized in terms of mineralogical composition, proximate analysis, morphology, and fuel-electrolyte interactions. These properties were then correlated with the electrochemical results obtained from open-circuit voltage (OCV) and linear sweep voltammetry (LSV) measurements. In addition, performance data from the literature, particularly from Kacprzak et al. [24,29], were directly compared with the results obtained in this study, allowing both validation of the experimental outcomes and extension of the comparative framework beyond a single set of fuels.

2. Materials and methods

2.1. Characterization of fuel

Table 1 shows the carbon-rich materials used as fuel in the MH-DCFC, their acronym and origin. Only Anthracite and Coke were fossil fuels; all other materials were biochars. The olive pomaces and Coke were already characterized by Dall'Osto et al. [25,30], in terms of mineralogical composition and proximate analysis.

The morphology of all the carbon-rich fuel particles was identified by means of Zeiss Sigma 300 Field Emission Gun Electronic Scanning Microscope (SEM). The aspect ratio (AR) of the particles was calculated according to ISO 9276-6 (see equation (1)), where a value of 0 indicates elongation and a value of 1 indicates sphericity.

$$AR = \frac{l_{min}}{l_{max}} \tag{1}$$

where l_{max} is the highest dimension of the particle and l_{min} the lowest. The porosity of the particles was instead calculated according to Refs. [31,32]. The darker spaces inside the SEM images detected using Otsu multi-level thresholding over gray-scale are considered as porous and they are measured using the algorithm Watershed.

All the materials were also chemically and mineralogically characterized by means of X-Ray Diffraction (XRD) through Rigaku SmartLab SE diffractometer in θ-θ configuration (Cu-Kα radiation: λ = 1.54 Å at 40 kV, 40 mA). The analysis was accomplished with a scan range of 5-90° 2θ through a 1D D/teX Ultra 250 detector featured by an XRF suppression filter; the powdered materials were scanned at 2° min^{-1} with a step size of 0.02° and rotated at 60 rpm.

The macro thermogravimetric proximate analysis was performed according to ASTM D7582-15 standard. The sample was initially heated at 105 °C for 1 h in inert environment (Ar) to calculate the moisture content (H_2O) according to equation (2).

$$H_2O = \frac{m_i - m_{105}}{m_i - m_c} * 100 \tag{2}$$

where m_i is the mass of the crucible containing the powder before the thermal treatment, m_c is the mass of the empty crucible and m_{105} is the mass of the crucible containing the powder after the thermal treatment at 105 °C.

The volatile matter (VM) was calculated heating the materials at 1000 °C for 15 min in inert environment (Ar) according to equation (3).

$$VM = \left[\left(\frac{m_{105} - m_{1000}}{m_{105} - m_c} * 100 \right) * \frac{100}{(100 + H_2O)} \right] \tag{3}$$

where m_{1000} is the mass of the crucible containing the powder thermally

Table 1
Materials used as fuel, their acronym and their origin. (The same olive pomace was pyrolyzed at 350 and 750 °C to produced OP350 and OP750, respectively).

Material	Acronym	Origin
Anthracite	Anthracite	
Coke	Coke	
Biochar	OP350	Olive pomace
Biochar	OP750	Olive pomace
Biochar	SS	Sewage sludge
Biochar	AGD	Agricultural digestate
Biochar	AGW	Agricultural waste
Biochar	WR	Wood residues
Biochar	OAC	Olive acquachar

treated at 1000 °C, m_{105} is the mass of the crucible containing the powder after the thermal treatment at 105 °C, H_2O is the moisture content and m_c is the mass of the empty crucible. Switching instead the atmosphere to air and keeping the material at 1000 °C for 15 min, the oxidation reaction allowed to quantify the ash according to the mass residue as described in equation (4).

$$\text{Ash} = \left[\left(\frac{m_{1000} - m^*_{1000}}{m_{1000} - m_c} * 100\right) * \frac{100}{(100 + H_2O + VM)}\right] \quad (4)$$

where m^*_{1000} is the mass of the crucible containing the powder thermally treated at 1000 °C in air, m_{1000} is the mass of the crucible containing the powder thermally treated at 1000 °C in inert atmosphere, VM is the volatile matter, H_2O is the moisture content and m_c is the mass of the empty crucible. The fixed carbon (FC) was then calculated according to equation (5).

$$FC = 100 - (H_2O + \text{VM} + \text{Ash}) \quad (5)$$

The total carbon C_{tot} was calculated by means of the Carbon elemental analyzer ELTRA's CS-580.

The wettability tests were conducted based on the sessile drop test described in BS EN ISO 1940 and ASTM D7334-08 (2017) standards. The contact angle was measured after a small amount of each powder was pressed into a disc shape and a drop of the electrolyte was deposited on its surface. Contact angle lower than 10° means super-electrolyte wettability, contact angles between 10 and 90° show electrolyte wettability while contact angles greater than 90° mean electrolyte nonwetting [33].

2.2. MH-DCFC design

The laboratory scale MH-DCFC, also used in a previous work [25], was employed to investigate the electrical performances of different carbon-rich materials according to their physicochemical properties. The trends reported for the properties correlation do not represent a mathematically derived model; rather, they are visual guides intended to illustrate the general behavior of the data. Consequently, these trends are not described by any analytical equation. The schematic design of the fuel cell is reported in Fig. 1.

In order to ensure a sufficient corrosion resistance over time against an alkaline environment, the crucible (Φ 85 × 135 mm) which acts as electrolyte container, was made in INCONEL 625. The inlet air tube was made by the same material and air was blown into the molten electrolyte at a rate of 10 NL h^{-1} at 1.6 bar. Furthermore, the tube was also used as cathode and respective current collector. The cell was heated at 450 °C by a band heater and thermally insulated by ceramic wool. For safety and handling reasons, the system was placed inside a steel container and the two systems were electrically insulated. The fuel was instead contained in a tea-bag made in stainless steel 316 (SS316) which acted as anode and the current collected thank to SS316 wire directly connected to the tea-bag. In order to avoid the leakage of the fuel from the tea-bag, the latter was surrounded by a metallic 200 mesh still in SS316. The anode and the cathode were electrically insulated by means of a ceramic cork. The electrolyte was a mixture of NaOH and KOH (80 wt% of NaOH and 20 wt% of KOH) to reduce the melting temperature of the pure NaOH to 290 °C [34]. A third hole on the cell cover allowed the evacuation of the gases produced.

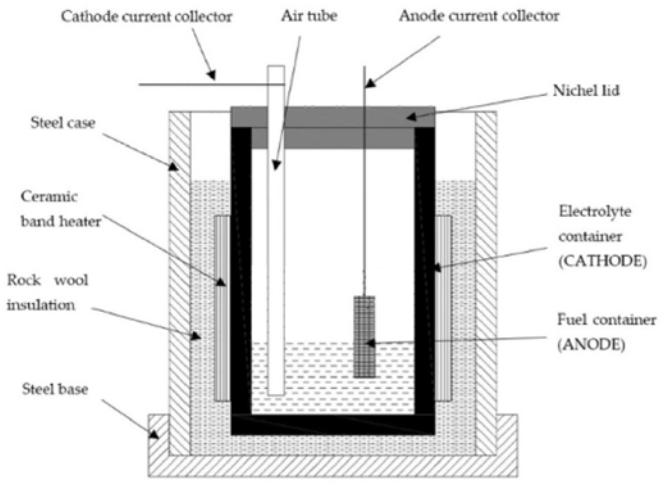

Fig. 1. Schematic representation of the MH-DCFC used.

2.3. Electrochemical measurements

The electrical analyses were performed on carbon-rich materials grounded and sieved to have their particle size distribution between 125 and 500 μm. In order to keep the same contact area of 11 cm^2, the volume (Φ 20 mm, height of 20 mm) of the fuel inside the tea-bag was kept constat. Due to different apparent fuels' density, the mass charged of each material is reported in Table 2.

To measure the MH-DCFC performance, an AMEL 2553 potentiostat, operated with its proprietary software VApeak 2018, was used. For the measurements, a two electrodes configuration was selected, with the anode working as the working electrode and cathode as the counter electrode. The Open Circuit Voltage (OCV) was monitored at 450 °C before each test and recorded until the potential stabilized for 500 s within ±5.0 mV. Once the stabilization was achieved, Linear Sweep Voltammetry (LSV) was performed by decreasing the potential from the stabilized OCV to 0 V. The scan rate of 2.5 mV s^{-1} was selected. A faster scan rate could exaggerate capacitive charging current and introduce distortions in the plotted curve, while a slower scan rate would improve accuracy [35], but drastically increases the time required for each analysis. All electrochemical measurements were evaluated as acquired, without applying normalization procedures to account for time-dependent corrosion effects on the cell itself. Data sets were included in the analysis only when stable and reproducible electrochemical responses were observed because considered representative of intrinsic fuel activity. Conversely, measurements exhibiting OCV values exceeding 1100 mV and showing poor reproducibility across repeated experiments were instead attributed to corrosion effects and discarded. Tests were also discarded when visible anode degradation after removal from the electrolyte or mechanical failure was observed.

3. Results and discussion

A prior characterization of the fuels tested inside a MH-DCFC was necessary because their physicochemical properties, e.g., chemical composition, presence of impurities, graphitization and surface area, strongly affect the reactivity of carbon to oxidation and the following electrochemical performances of the fuel cell [36,37].

Table 2
Mass of each fuel used to guarantee the same contact area.

Material	Mass used [g]
Anthracite	4.028
Coke	5.486
OP350	2.305
OP750	2.212
SS	2.801
AGD	3.857
AGW	2.538
WR	1.208
OAC	2.305

3.1. Fuel characterization

3.1.1. Particle size distribution

Fig. 2 shows the visual appearance of all the carbon-rich materials used as fuel in the MH-DCFC and their morphology.

The dimension, aspect ratio and the porosity of the particles are reported in Table 3. Anthracite, AGW and AGD showed the finest texture, whereas Coke consisted of particles easily visible to the naked eye. OP350 and OP750 had a very similar appearance and particle size, as they originated from the same raw material pyrolyzed at different temperatures. SS exhibited a sludgy appearance, consistent with its origin. OAC was composed of elongated particles resembling agricultural residues. The fibrous shape was typical of biomass derived from agricultural waste, with an irregular surface and non-uniform cross section. The smoothness and the fine surface texture are representative of most fibers isolated from plant stems [38]. WR indeed showed a similar appearance characteristic of wood residue, despite the fragments were bigger in dimension. On the contrary, AGW seemed finer and made of more circular particles. The porosity of the bio-residues fitted within the expected range of 7.41-60.65%, typical for biochar [39], and also the porosity of Anthracite (2.16%) was consistent with the one defined in the literature as being lower than 10% [40].

Table 3
Mean dimension, aspect ratio and porosity of carbon-rich fuel particles.

Materials	Dimension [μm]	Aspect ratio	Porosity [%]
Anthracite	227.34 ± 37.86	0.880 ± 0.111	2.16
Coke	389.02 ± 144.89	0.808 ± 0.174	29.97
OP350	327.07 ± 143.19	0.568 ± 0.166	33.07
OP750	335.30 ± 122.99	0.664 ± 0.254	30.78
SS	364.46 ± 139.56	0.713 ± 0.069	12.83
AGD	212.30 ± 60.73	0.709 ± 0.177	13.35
AGW	205.61 ± 71.91	0.538 ± 0.149	18.62
WR	496.52 ± 265.56	0.369 ± 0.129	42.72
OAC	380.34 ± 240.69	0.537 ± 0.266	24.38

3.1.2. Mineralogy

The XRD pattern of each fuel is reported in Fig. 3. The majority of fuels were characterized by the presence of broad valley of carbon identified as amorphous [41]. The only exceptions were Anthracite and Coke which presented higher graphitization (83 and 27% respectively,

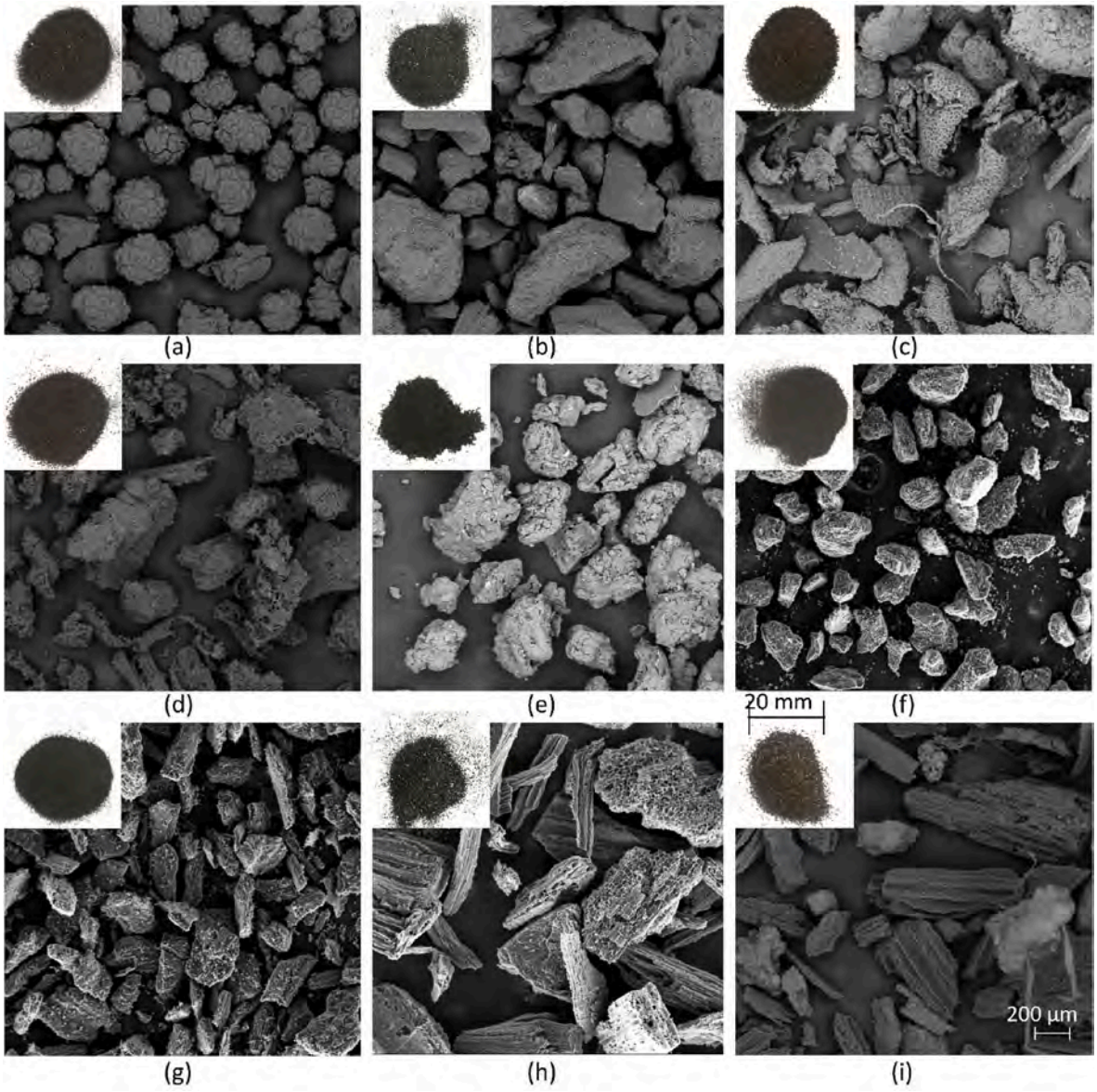

Fig. 2. Visual appearance and SEM images of carbon-rich materials a) Anthracite; b) Coke; c) OP350; d) OP750; e) SS; f) AGD; g) AGW; h) WR; i) OAC.

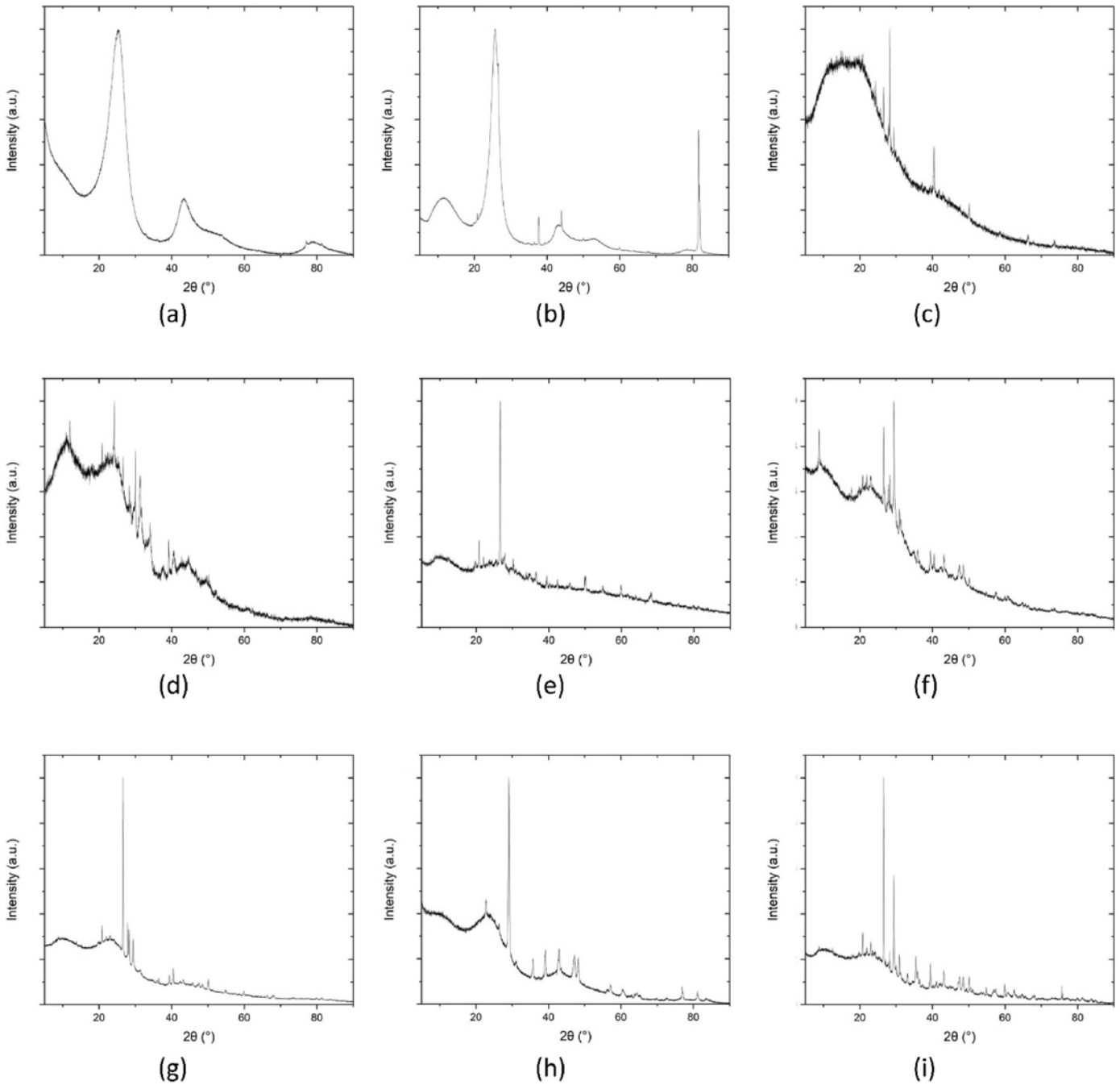

Fig. 3. XRD pattern of a) Anthracite; b) Coke; c) OP350; d) OP750; e) SS; f) AGD; g) AGW; h) WR; i) OAC.

calculated according to Wang et al. [42]). The mineralogical analysis (detailed mineralogical characterization is provided in supplementary materials) identified that only Anthracite was made of solely graphite. It was therefore used as the standard for comparing the electrical properties of the MH-DCFC produced using different carbon-rich materials. All the other fuels were instead made up of impurities. The effects of their presence were hence investigated to understand how they could influence the OCV and LSV. For instance, quartz (SiO_2) and calcite ($CaCO_3$) were present in mostly each material. SiO_2 was not identified only in WR, while $CaCO_3$ in Coke and SS. Another common phase was sylvite (KCl), identified in OP750, OP350, AGD and ADW. The pyrolysis at low temperature caused the presence of residual hemicellulose in OP350, requiring higher temperature to be completely pyrolyzed [43], while kalicinite ($KHCO_3$) was identified in OP750. SS and OAC contained some iron oxides such as hematite (Fe_2O_3) and magnetite (Fe_3O_4), respectively.

3.1.3. *Proximate analysis*

The macro thermogravimetric proximate analyses of each carbon-rich material used as fuel in the MH-DCFC are reported in Table 4. The proximate analysis of SS was also calculated on the dry-base material (SS*db) due to its high initial moisture. When the fuel was immersed in the hot electrolyte, the moisture immediately evaporated. Therefore, the actual available VM, FC and ash content in the material were not the real one, but the values reported as SS*db. However, due to the uncertainty of this assumption, the following correlation between the electrochemical performances and the chemical properties would take into consideration both SS and SS*db. The same methodology was

Table 4
Macro thermogravimetric proximate analysis of each fuel. (H_2O refers to the moisture content, VM is the volatile matter fraction, FC is the amount of fixed carbon; C_{tot} is the total carbon) (SS*db was calculated drying the fuel due to the high moisture content in the raw material).

Material	H_2O [wt. %]	VM [wt. %]	FC [wt. %]	Ash [wt. %]	C_{tot} [wt. %]
Anthracite	1.05	1.69	92.66	4.60	94.35
Coke	0.05	5.20	85.20	8.60	87.50
OP350	2.12	61.32	20.79	15.85	65.23
OP750	2.72	50.49	30.29	16.50	69.87
SS	24.45	18.48	15.92	41.15	22.63
SS*db	-	24.46	21.07	54.47	29.95
AGD	3.60	14.67	50.23	31.50	53.20
AGW	3.00	15.99	57.52	23.49	62.46
WR	5.93	10.64	74.63	8.79	83.66
OAC	2.67	23.21	44.89	29.23	68.09

not performed for other fuels because they did not exceed the 5 wt% of moisture.

3.1.4. Wettability

The interactions between the electrolyte and the fuels are shown in Fig. 4.

Both OP350 and OAC reacted immediately upon contact with the electrolyte. Therefore, it was not possible to evaluate the contact angle due to the formation of an irregularly shaped bubble. Anthracite had contact angle of 104.52°, AGW 109.95° and AGD 140.315°. These latter showed non-wettable behaviour. OP750 and SS instead exhibited a good electrolyte wettability having contact angles of 44.31 and 56.82°, respectively. In addition, the bubble of electrolyte poured on their surface remained bright without attracting the fuel's powder, as instead happened in case of electrolyte-non wetting surface. Despite the wettability due to a contact angle of 62.51°, Coke was dragged by the electrolyte covering the bubble, behaving like a non-wettable material [44]. The limiting condition in term of contact angle was WR which was characterized by an angle of 87.11° and, as in the previous case, the bubble was completely covered by the carbon-rich material. The amount of fixed carbon affected the fuel's capacity to be attracted by the electrolyte. Indeed, the carbon-rich materials with limited FC (OP350 O750, SS and OAC had 20.79, 30.29, 15.2 and 44.89 wt%, respectively) were not attracted to the bubble, unlike the other fuel which contained a minimum of 50.23 wt%.

3.2. Open circuit voltage

A fuel cell is defined as perfect working when the open circuit potential is equal to the reversible potential, and in case of DCFC operating at 450 °C the theoretical OCV is 1025 mV [24]. However, the experimental results obtained when testing the different carbon-rich materials inside an MH-DCFC, shown in Fig. 5, differed according to the fuel used, in terms of both the potential value reached and the time taken to stabilize it.

The observed fluctuations in potential were attributed to the corrosion of the SS316 used to construct the anode. This increased the cell's electrical resistance and worsened the electron charge collection [45]. In addition, Cherepy et al. [36] found that voltages below 600 mV could not sustain a constant power condition, which could explain why the OCV curve of Anthracite was fragmented and spiked. Concurrently, WR was the only carbon-rich material that did not appear to activate as evidenced by the voltage drop to 40 mV after 3000 s. Furthermore, once the anode was removed WR appeared clustered inside the tea-bag, losing its original powder nature. The agglomeration of the fuel is an intrinsic limitation of the DCFC performance, as the reduction in surface area means there are fewer opportunities for electrochemical reactions between the electrolyte and carbon [46]. For this reason, WR was no further taken into consideration in this work.

3.2.1. Effect of wettability

Fuel cells rely on electrochemical interfacial interactions between the liquid electrolyte and the solid fuel [47]. Wettability of the powder surface by the electrolyte is thus a critical factor as it determines whether the interaction at the interface happens and how efficient the interaction is. A greater wettability can be a good indicator of whether a specific fuel will generate a good power density [33], because the wettability of the electrode determines the active region area in contact with the electrolyte [44]. In addition, the wettability is a key parameter to affect the stability of operation in short-term and the lifetime in long-term operations [44]. However, the initial period of the OCV curves could be associated with the gradual wetting of the fuel by the liquid electrolyte [24]. Indeed, although most of the sessile drop tests indicated non-wettability between the fuels and the electrolyte (Fig. 4), once immersed the complete transition from non-wetting to wetting of the meniscus can occur within a few hours with a following CO release and increase in the OCV, as observed by Cooper et al. [48]. Therefore, this transition could explain why a non-wettable fuel, such as AGW, took 5760 s to stabilize. Another factor affecting the stabilization time was the fuel's tendency to adhere to the electrolyte. Despite their initial wettable or non-wettable behavior, OP750, SS and AGW required more time to stabilize than Anthracite, Coke and AGD (3060, 4320, 5760, 1200, 1680 and 2520 s, respectively), because the particles attached to the electrolyte. This increases the relative contact between the particles and the electrolyte, thereby improving the reaction kinetics. The strong interaction between OP350, OAC and electrolyte did not affect the kinetic, since OP350 required 3000 s to stabilize its potential, whereas OAC only needed 840 s. However, this strong reactivity between the fuel and the electrolyte could be responsible for their initial decrease in

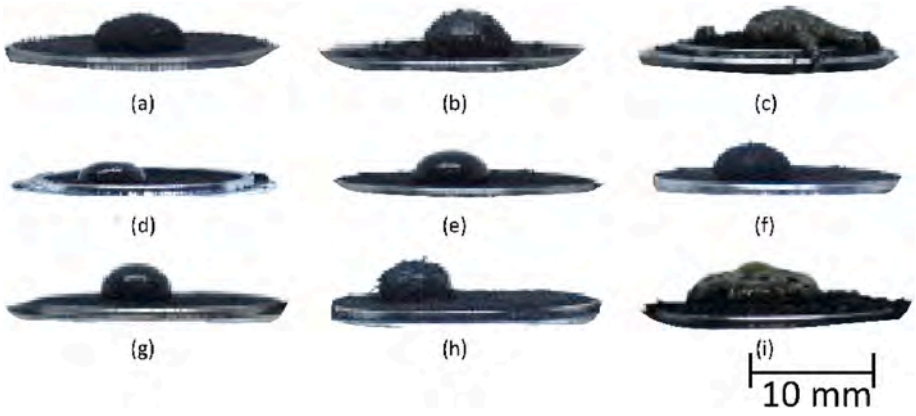

Fig. 4. Sessile drop to define the interaction between electrolyte and fuel a) Anthracite; b) Coke; c) OP350; d) OP750; e) SS; f) AGD; g) AGW; h) WR; i) OAC.

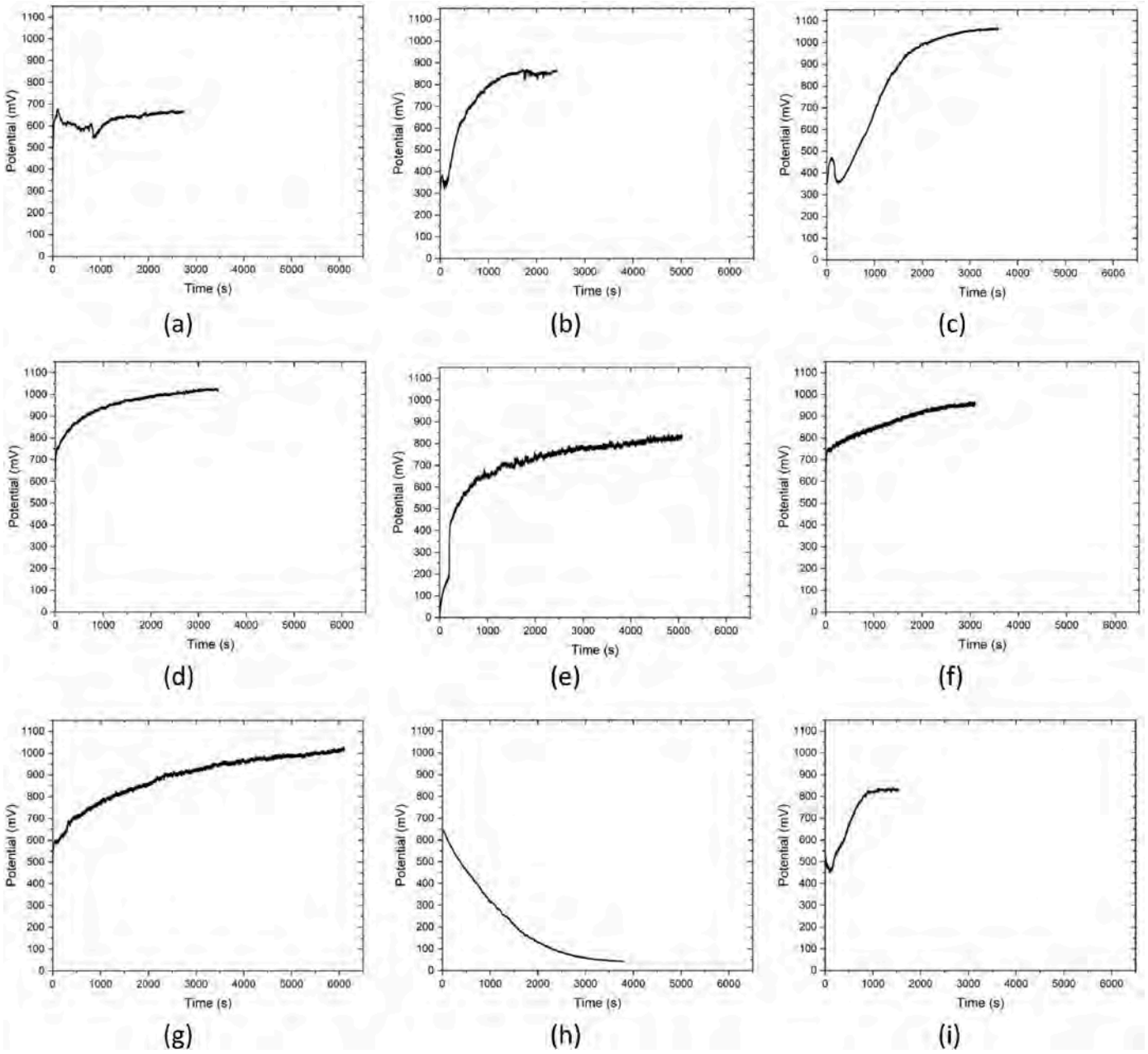

Fig. 5. OCV curves of a) Anthracite; b) Coke; c) OP350; d) OP750; e) SS; f) AGD; g) AGW; h) WR; i) OAC.

potential, causing a rapid consumption of the volatile matter and resulting in an initial loss of performance. Kacprzak et al. [29] demonstrated the same phenomenon and explained it as the degassing of coal particles after immersion in the molten electrolyte.

3.2.2. *Effect of graphitization*

The graphitization of the carbon also affected the stabilization of the OCV. Graphitic carbons as Anthracite and Coke, were typically very conductive, enhancing hence the charge transport and reaching stabilization in short time. However, they were less chemically reactive, as depicted by the limited OCV values compared to the less graphitized biochar (Fig. 3) [36]. Consequently, the reactivity is more important than high electrical conductivity in DCFC [49], because the electrical conductivity of the fuel is a marginal parameter when the current collector is not made of carbon itself [27].

3.2.3. *Effect of aspect ratio*

The aspect ratio of the fuel's particles was a further parameter which directly affects the stabilization time of the OCV. Fig. 6a shows that a more regular shaped particles as Anthracite (aspect ratio closer to 1) required less time to stabilize than elongated particles as AGW (AR = 0.538). The presence of irregularly shaped particles (with an aspect ratio closer to 0) could act as an electrode in a battery, where the viscosity of the slurry increases due to the increased friction and interlocking of the particles. Indeed, high-viscosity slurry limits the coating process and the ion transfer rate [50]. The presence of elongated particles in the MH-DCFC could therefore cause the same delay, resulting in a longer stabilization time for the OCV, since the particles' arrangement inside the tea-bag is limited by friction. However, the fine irregular shape increases the particle-liquid interaction, due to high surface area [50], resulting in higher OCV than that of more regular shape particles (Fig. 6b). The high value was therefore due to the better adhesion of the elongated particle to the tea-bag wall, which promoted electron transfer

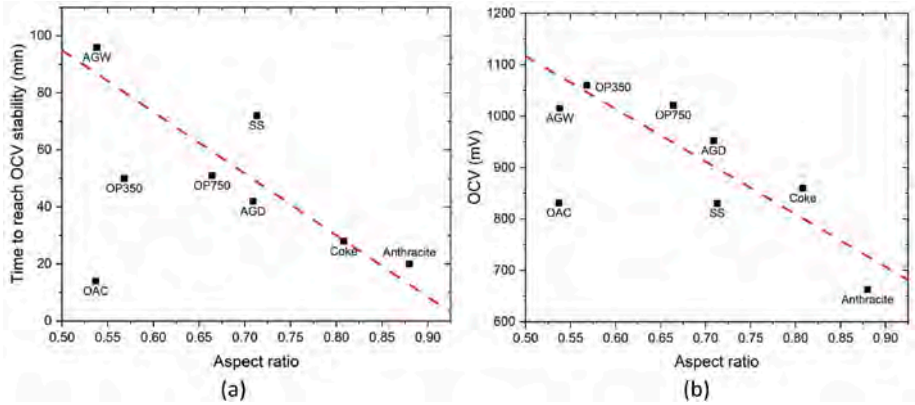

Fig. 6. a) Time required to reach the OCV as a function of the particles' fuel aspect ratio. b) OCV as a function of the particles' fuel aspect ratio.

[51]. Despite appearing as an outlier based on its value (0.537), OAC fits well within the curves when the AR standard deviation (0.266) is taken into account, indicating that its deviation is consistent with the expected variability of the trend rather than representing a true anomaly.

3.2.4. *Effect of volatile matter*

Fig. 7 shows that the OCV increased as the volatile matter content increased, reaching a plateau at nearly 30 wt% VM. This increasing trend up to 40 wt% was also confirmed by the values obtained by Kacprzak et al. [24,29]. According to this evidence, it is reasonable to hypothesize that the reaction predominantly proceeds via gasification processes, effectively exploiting the volatile matter released from the fuel, which subsequently plays a key role in sustaining the electrochemical activity. Although in the DCFC the gasification is not a separate step, the slow kinetic of direct oxidation of the solid carbon could favor such an alternative mechanism [52].

Volatile matter was primarily responsible for the rapid carbon activation, which explains the need for a fuel rich in VM [12]. However, a certain fraction could be immediately consumed at the beginning of the test. For instance, OP350 released a high amount of fume which is typical for the volatilization of the gaseous compound when the fuel was immersed in the electrolyte [29]. This phenomenon was also due to the strong reactivity with the electrolyte shown in Fig. 4. Indeed, a high fume release also occurred with OAC, which has the same strong interaction shown by OP350-electrolyte.

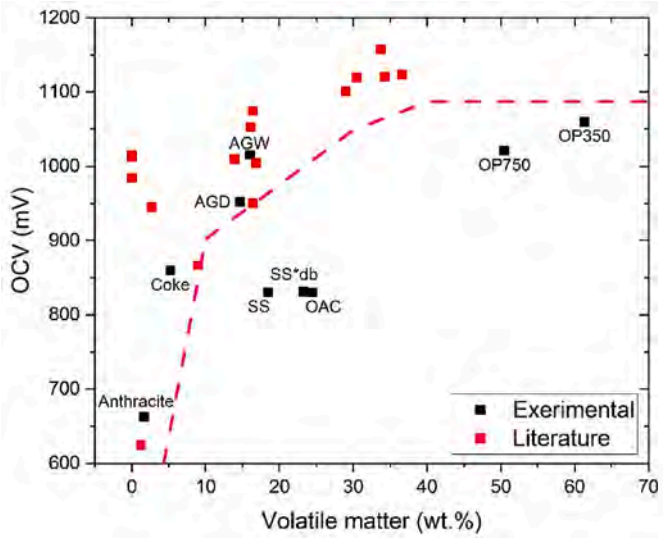

Fig. 7. OCV as a function of volatile matter. Black points represent the experimental data collected by the author, while red points indicate literature data gathered from the literature review (Kacprzak et al. [24,29]). (For interpretation of the references to colour in this figure legend, the reader is referred to the Web version of this article.)

In particular, OP350 got an OCV higher than the theoretical value (1060 vs 1025 mV) due to some alternative reaction mechanism whereby compounds could be chemically oxidized in the cell [13,24,53]. Furthermore, a disordered form of carbon, as the residual hemicellulose present after the pyrolysis at 350 °C, was responsible for higher electrochemical performances [36,37].

The main anodic reaction and the main source of electrons generation inside a MH-DCFC is the electrochemical oxidation of carbon [7] reported in equation (6)

$$C + 4OH^- \rightarrow CO_2 + 2H_2O + 4e^- \quad (6)$$

This reaction was probably further stimulated in OP350 by the presence of hemicellulose, which provide further OH^- groups. Additionally, the oxygen and hydrogen present in the hemicellulose are two of the main mediators that significantly contributed to oxidation and increased the theoretical open circuit voltage [13]. The concentration of H_2 hence plays a crucial role because its oxidation can further produce electricity [54]. Kawase et al. [55] highlighted an increase of potential of 28.57% increasing the hydrogen concentration to 20%. Lee et al. [56] indeed explain that the high number of H_2 present in the phases could increase the OCV over the theoretical value (1050 mV at 850 °C) due to the oxidation with positive reaction order. This can be mathematically calculated being the potential calculated via Nerst equation directly dependent on the partial pressure of H_2 [56].

Additionally, other alternative processes of power generation could take place simultaneously (equation (7)) [28], contributing to the overall cell performance and affecting the OCV the reaction [52]. Partial oxidation of carbon leads to the formation of carbon monoxide which would be further oxidized within the anodic compartment at higher over potentials [57]. The change in dominant mechanism to the overall carbon oxidation into two stages leads to an increase of OCV [58]. On the contrary, the only partial oxidation of carbon (equation (7a)) causes low thermodynamic efficiency [54].

$$\begin{aligned} &a)\ C + 2OH^- \rightarrow CO + H_2O + 2e^- \\ &b)\ CO + 2OH^- \rightarrow CO_2 + H_2O + 2e^- \end{aligned} \quad (7)$$

However, the progressively consumed VM during the test makes impossible to work with highly volatile material. A sufficient amount of fixed carbon is also required, although it takes more time to activate. This explains why increasing the VM to 40 wt% did not result in any further increase in the OCV.

3.2.5. *Effect of fixed carbon*

Fig. 8a shows that the OCV increased with an increase in fixed carbon up to a content of 40-50 wt%, after which the OCV decreased.

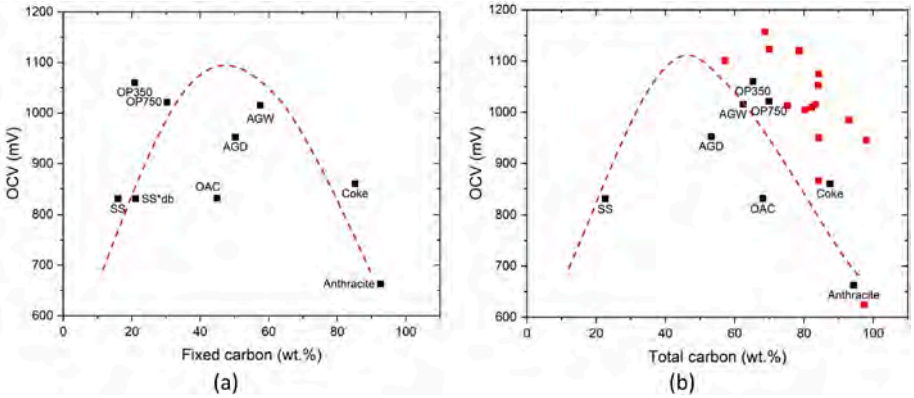

Fig. 8. a) OCV as a function of the fuels' fixed carbon content; b) OCV as a function of the fuels' total carbon content. Black points represent the experimental data collected by the author, while red points indicate literature data gathered from the literature review (Kacprzak et al. [24,29]). (For interpretation of the references to colour in this figure legend, the reader is referred to the Web version of this article.)

On the one hand, a low amount of FC did not provide the necessary carbon for the electrochemical reaction after the progressive consumption of VM in the fuel. On the other, a high concentration of FC limited the presence of VM, meaning the fuel would take a longer time to activate in the cell. The negative effect of high amount of carbon was also confirmed by Kacprzak et al. [24,29] (Fig. 8b), where the increase of total carbon caused a decreasing in the OCV. After the pyrolysis of a biochar, the total carbon is indeed associable with the fixed carbon [59].

3.2.6. *Combined effect of volatile matter and fixed carbon*

The previous results suggested that a balance was required between VM and FC to achieve a high OCV. Fig. 9a indeed shows that a maximum in OCV was achieved using a carbon-rich material with a FC/VM ratio of 1-2. The data collected by Kacprzak et al. [24,29] (Fig. 9b) also highlighted a maximum using a fuel with 1-2 C_{tot}/VM. This confirmed that an excess of either VM or C_{tot} negatively affects the OCV of the chemical reaction. At least 2 FC/VM ratio is required for better electrochemical performance. Kacprzak et al. [53] indeed noticed that an excess of VM could potentially disrupt the electrochemical reaction in the anode. However, excess of FC could necessitate higher temperature and longer activation time [12].

3.2.7. *Effect of ash*

Although, the amount and the chemical composition of the ash were also factors affecting the OCV, Fig. 10a shows that an ash content of up to 25-30 wt% did not negatively affect the OCV. Additionally, fuels with a limited ash content were considered more advantageous for enhancing the DCFC performances [53,14]. A low ash content could indeed favor the reaction, since ash may react with the electrolyte. For example, compounds rich in hydrogen and oxygen, like $Ca(OH)_2$ (which further decompose to CaO and H_2O at 450 °C as shown in equation (9)) due to the reaction between $CaCO_3$ and NaOH [60,61], were most probably produced during the oxidation of the fuel, which improved the cell performance [26]. On the other hand, the OCV decreased linearly as the ash content increased by over 25 wt%, due to progressive carbon consumption during the test causing ash to accumulate on the anode surface and consequently reducing performance, by acting as a physical barrier for the active site of the carbon [53,62]. Furthermore, not only did the relative ratio between carbon and ash increased during the analysis due to consumption of the former, but an initial excessive presence of ash further enhanced this drawback.

The origin of the fuels also affected the electrochemical properties. Biochar derived from agricultural waste exhibited higher potential values (OP350: 1060 mV, OP750: 1021 mV and AGW: 1015 mV) than fossil (Anthracite: 662 mV). Similar results were obtained by Kacprzak et al. [24], who did not exceed 600 mV using a fossil graphite rod, whereas once biochar was used as fuel it achieved an OCV of 1050 mV. This was due to the presence of catalytic compounds inside the biochar's ash, which favored the electrochemical reaction (e.g., $CaCO_3$, Fe_2O_3, KCl) [26]. On the contrary, OCVs lower than the theoretical value (OAC: 831 mV, Anthracite: 662 mV, Coke: 860 mV, AGD: 952 mV and SS: 830 mV) were due to incomplete oxidation of solid carbon [13].

For instance, although a high ash concentration and a no-favorable FC/VM ratio, SS and OAC got an OCV better than that of fossil coals. Both contained some iron oxides (Fig. 3), which acted as a catalyst [37,63]. Iron oxide is indeed the best-known catalyst for carrying out carbon

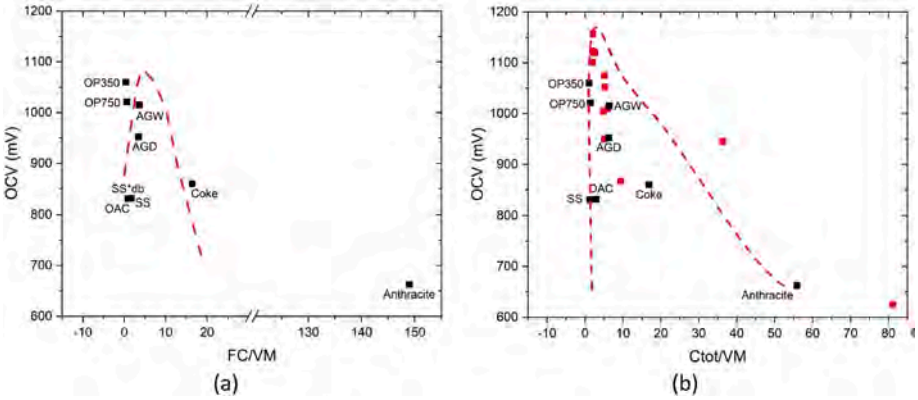

Fig. 9. a) OCV as a function of the ratio between fixed carbon e volatile matter. b) OCV as a function of the ratio between fixed carbon e volatile matter. Black points represent the experimental data collected by the author, while red points indicate literature data gathered from the literature review (Kacprzak et al. [24,29]). (For interpretation of the references to colour in this figure legend, the reader is referred to the Web version of this article.)

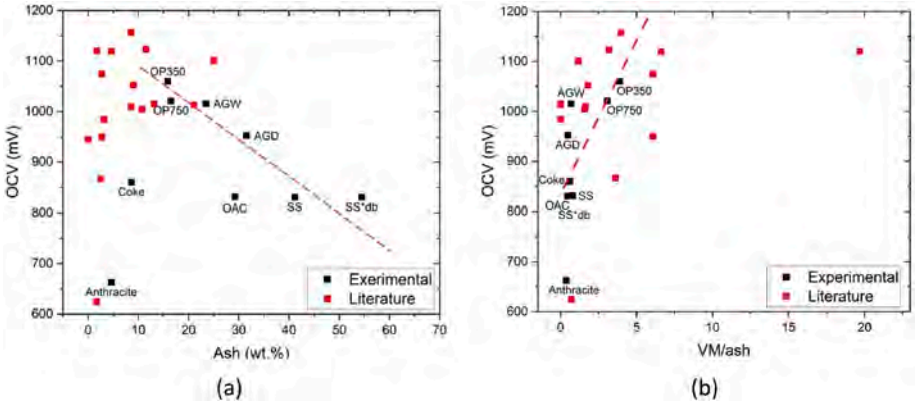

Fig. 10. a) OCV as a function of ash content in the fuels; b) OCV as a function of the ratio between volatile matter and ash. Black points represent the experimental data collected by the author, while red points indicate literature data gathered from the literature review (Kacprzak et al. [24,29]). (For interpretation of the references to colour in this figure legend, the reader is referred to the Web version of this article.)

gasification at low temperatures and catalyzing the reverse Boudouard reaction [62]. In addition, the presence of the iron oxides directly incorporated inside the biochar guarantee its direct contact with carbon, which could be instead limited in case of mechanical mixing [63].

Although the reaction mechanism at the anode is very complex and unknown [57], the different mineralogical phases identified in the XRD analysis (see Supplementary Material) could react with the electrolyte, leading to the formation of other species. As the electrolyte is a mixture of 20 wt% KOH and 80 wt% NaOH, only the latter is considered in the discussion. Considering the most abundant phases and trying to list the possible reactions as a function of the abundance of a specific compound in the fuels, the following equations reported the main reactions involved. It is worth mentioning that further interactions among the reaction products were not considered. Moreover, only spontaneous reactions ($\Delta G < 0$) at the working condition (450 °C) were reported. Free Gibbs energy of formation for products and reagents was determined from Barin [64].

$$SiO_2 + 2NaOH \rightarrow Na_2SiO_3 + H_2O \ (\Delta G_r = -124\ kJ/mol) \quad (8)$$

$$CaCO_3 + 2NaOH \rightarrow Na_2CO_3 + Ca(OH)_2 \rightarrow Na_2CO_3 + CaO + H_2O(\Delta G_r = -42\ kJ/mol) \quad (9)$$

$$Al_2Si_2O_5(OH)_4 \rightarrow Al_2Si_2O_7 + 2H_2O \rightarrow Al_2Si_2O_7 + 6NaOH \rightarrow 2NaAlO_2 + 2Na_2SiO_3 + 3H_2O(\Delta G_r = -381\ kJ/mol) \quad (10)$$

$$(C_6H_{10}O_5)_n + 12NaOH + H_2O \rightarrow 6Na_2CO_3 + 12H_2\ (\Delta G_r = -1210\ kJ/mol) \quad (11)$$

$$(C_5H_8O_4)_n + 10NaOH + H_2O \rightarrow 5Na_2CO_3 + 10H_2(\Delta G_r = -915\ kJ/mol) \quad (12)$$

The reaction (10) is written for Kaolinite, but it is extensible for all the clays (illite $KAl_2(AlSi_3O_{10})(OH)_2$, annite $KFe_3AlSi_3O_{10}(OH)_2$ and muscovite $KAl_2(AlSi_3O_{10})(OH)_2$).

When in large amounts, the reaction between quartz and the electrolyte (8) could lead to the formation of a passivating membrane of M_2SiO_3 (where M is either K or Na) on the anode, limiting current flow and carbon oxidation [65]. The passivation or inhibitive effect of SiO_2 on the electrode might limit the cell performances [12,27,37]. This seems confirmed by the stabilization of OCV and power density around 900 mV and 4 mW cm^{-2}, respectively, after 0.6 g as absolute mass of ash in the fuel. High absolute mass of ash means high quartz concentration in the system, given that quartz is present as main ash compound in all the tested chars.

The other reactions, differently, give to the formation of Na_2CO_3 which is responsible for chemical instability in MH-DCFC due to electrolyte degradation [66]. However, these drawbacks are balanced by the positive effect of water generation. The amount of water generated by reactions 8, 9 and 10 improved the cell performance because H_2O limits the formation of further carbonates in the electrolyte [7,7,67,68]. The working temperature was indeed too low to favor the reverse Boudouard reaction [7,28,67]. Therefore, the produced CO_2 via equation (6), could react with the hydroxide group according to (13), if not discharged in time [69], causing the degradation of the electrolyte and shorting the cell operation [67]. Water inhibits reaction (13) by complexing carbonate group according to (14) [70], hence suppressing the carbonation of the electrolyte, also liberating additional electrons responsible of registered overpotentials.

$$2OH^- + CO_2 \rightarrow CO_3^{2-} + H_2O \quad (13)$$

$$6OH^- + C \rightarrow CO_3^{2-} + 3H_2O + 4e^- \quad (14)$$

Although the precise mechanism of how the water is able to mitigate this effect is unclear [7], Gurbuz et al. [68] demonstrated that dissociation of hydroxides is effectively prevented.

Additionally, water reduces the anode degradation because it increases the ionic conductivity of the melt and reduces the iron corrosion [54,57]. Finally, H_2O is a necessary component for the H_2 oxidation and the following increase in the OCV. The highest OCV was indeed obtained by OP350 which contains both quartz and hemicellulose (whose main components are xylan $(C_5H_8O_4)_n$ and glucomannan $(C_6H_{10}O_5)_n$), the former responsible for H_2O liberation and the latter for H_2 liberation.

Finally, KCl (found in OP350, OP750, AGD and AGW) although it does not react with the electrolyte (its reaction is in dynamic equilibrium with ΔG_r slightly positive) it may influence positively the reactivity of char because sylvite is one of the enhancers for carbon activation. KCl does not act directly as an activating agent, but promotes the solubilization of secondary products enhancing the contact of KOH and carbon particles, therefore increasing the activation efficiency [71].

On the contrary, $KHCO_3$ does not provide any beneficial or detrimental effect, since it decomposes to K_2CO_3, hence bringing further carbonate to the electrolyte, and H_2O, whit its beneficial contribution.

3.2.8. *Combined effect between volatile matter and ash*

Concurrently, VM counterbalanced the negative effects of ash. As can be seen in Fig. 10b, an increase in VM/ash was correlated with a linear increase in OCV. Despite the progressive consumption of the volatile matter, an initial high VM/ash ratio favors the presence of active sites, favoring the electrochemical reaction. The data collected from the literature [24,29] confirmed that VM burns faster and is more reactive,

hence it is probably less affected by ash.

3.3. Linear sweep voltammetry

The curves obtained from the LSV and the corresponding characteristic values, such as power density and limiting current density, are reported in Fig. 11 and Table 5, respectively. The limiting current density and power density differed according to the type of fuel used, although the shape of the curves was similar among all tested coals. Furthermore, the power density values obtained in this work were in good agreement with the results of Kacprzak et al. [45], who achieved 4.8 mW cm^{-2} with biochar and 6.7 mW cm^{-2} with graphite using a comparable setup with an SS316 anode coupled to a Ni-alloy cathode and container. The similarity in both the cell materials and configuration explains the consistency in the observed electrochemical performance.

All the curves showed an initial limited voltage decrease associated to the activation resistance, then there was linear middle region characteristic of the ohmic resistance which is affected by electrolyte resistance, current collector resistance and carbon resistivity. Both Anthracite and OAC showed a further decrease in potential over 300 and 500 mV, respectively. In addition, slight variations in current were observed, which are characteristic of concentration polarization [24, 37]. The concentration polarization at the anode is negligible because in DCFC there is always an excess of carbon [70]. Therefore, the

Table 5
Limiting current density and power density of a) Anthracite; b) Coke; c) OP350; d) OP750; e) SS; f) AGD; g) AGW; h) WR; i) OAC.

Material	Limiting current density [mA cm^{-2}]	Power density [mW cm^{-2}]
Anthracite	4.82	1.67
Coke	4.82	2.49
OP350	12.41	5.04
OP750	10.24	5.46
SS	6.97	3.54
AGD	9.07	4.83
AGW	13.45	6.22
OAC	7.73	4.20

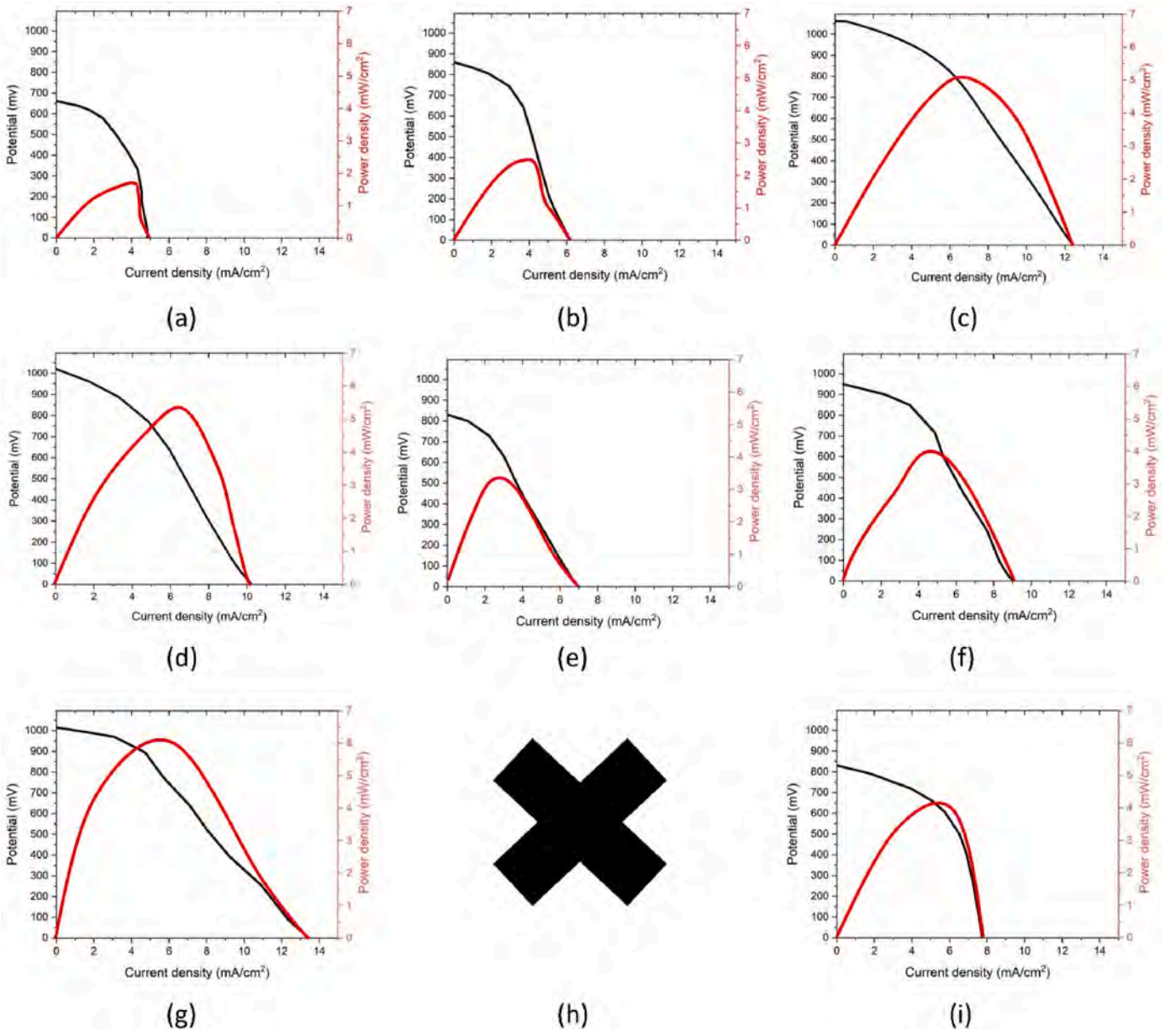

Fig. 11. LSV curves of a) Anthracite; b) Coke; c) OP350; d) OP750; e) SS; f) AGD; g) AGW; h) WR; i) OAC.

performance of the cell was limited [72] by the cathode concentration polarization due to a partial pressure of gases at the interface lower than in bulk gas phase [67]. Therefore, during the test, there was insufficient partial pressure of the active and useful gases. This resulted in the fuel being fully oxidized and fuel starvation occurring. This phenomenon could be associated to the properties of the fuel itself. Although OAC may contained some compound as hydrocarbons which were not fully evolved from the fuel during its carbonization [24], the strong interaction with the electrolyte may cause a fast consumption in the VM which resulted too low to sustain the electrochemical reaction. Indeed, the concentration polarization was also shown by Anthracite and Coke, which do not exceed 5.2 wt% of VM. The available gases are hence fast consumed and the temperature at which the test was performed and the limited time did not allow the complete activation of FC [12]. Kacprzak et al. [45,73] also obtained a lower reactivity for fossil fuel than biochar.

SS also exhibited concentration polarization, likely due to the substantial moisture content of the sample. The water immediately turned to steam when it came into contact with the heated electrolyte (450 °C), which further accelerated the test running out of gas.

3.3.1. Effect of volatile matter

Fig. 12a highlighted an increase of power density until 30-40 wt% VM, confirmed also by the data collected by Kacprzak [24,29] (Fig. 12b). The importance of VM was also confirmed by Jiang et al. [12] who explained that high volatile matter is synonymous of high generated power. Since the tests performed in this study took no longer than 2 h, the VM was primarily responsible for the results obtained [12]. The overall efficiency of the DCFC is indeed mainly due to gas-active electrochemical zone interactions rather than the pure carbon-active electrochemical zone contact [27].

Unfortunately, the small amount of data did not allow to confirm whether a VM greater than 40 wt% would result in a plateau or a decrease in performance. However, the hypothesis of a decrease in power density could be related to the volatilization of the VM, followed by the consumption of the material involved in the reaction. When the fuel was immersed in the electrolyte and heated, the coal structure changed and gases were produced. Therefore, due to the loss of these gases, most of the volatile coal fuel was lost from the cells, making it impossible to sustain longer the power [12]. It was hence impossible to use 100 wt% volatile carbon fuel. Indeed, a hydrochar containing 0.66 wt% of FC ad 66.80 wt% VM gave a limited power density compared to other material with lower VM [25].

3.3.2. Effect of fixed carbon

According to that, a sufficient amount of fixed carbon was necessary in the fuel. Indeed, Fig. 13a shows an increase in power density until 40-50 wt% FC, with a following decrease.

The same decrease in potential was observed when considering the data collected for total carbon content higher than 50 wt% by Kacprzak et al. [24,29] (Fig. 13b). Fuente-Cuesta et al. [13] also observed a decrease in power density from 67.5 to 45.2 mW cm^{-2} by increasing the carbon content from 89.6 to 93.1 wt%, respectively. As previously mentioned, a low carbon content hindered the electrochemical reaction, which instead was necessary for electron transfer after the volatile matter has been consumed. The problem with biochar containing a low amount of fixed carbon is that it generates a low amount of CO and CO_2 in situ at the anode compartment. This subsequently limits the extent of the electrochemical reactions of CO within the anode of the DCFC [27]. On the contrary, an excessive amount of fixed carbon would require a higher temperature and more time to be activated [12]. An improvement of the Anthracite electrochemical performances (OCV of 1100 mV and power density of 47.78 mW cm^{-2}) was indeed obtained by Jiang et al. [74] using a SOFC at higher temperature and longer time (750 °C in 2 h).

3.3.3. Combined effect between volatile matter and fixed carbon

The influence of VM and FC on the power density suggested that a balance between the two was required, as shown in Fig. 14 where a maximum in power density is shown around 1-2 FC/VM ratio. This maximum also indicated a decrease in power density at a VM greater than 40 wt%, further excluding the presence of a plateau. Considering the maximum identified in figure, the ideal chemical composition of a fuel should be an equal or maximum double content of FC respect to VM. Chien et al. [75] also defined that a medium volatile content is the more appropriate amount to use a biochar as fuel in DCFC. On the contrary, Grioui et al. [27] showed that FC/VM ratio closer to 1 negatively affected the cell results. The power density decreased by one order of magnitude using a fuel with 0.897 instead of 0.245 FC/VM ratio. This suggests the need of considering also other fuel characteristics (e.g., ash composition, morphological characteristics) to understand the reason behind their electrochemical behavior.

3.3.4. Effect of ash

A comparison of the results obtained by the authors (Fig. 15a) and those obtained by Kacprzak et al. [24,29] (Fig. 15b), showed a peak in power density occurred below 30 wt% ash. Jiang et al. [45], obtained the same trend, observing an increase in power using a hybrid SOFC with different fuels up to 15 wt% ash, followed by a decrease in performance.

3.3.5. Combined effect between ash, fixed carbon and volatile matter

Fig. 16a also confirms the negative effect of ash on cell performance, since power density increased as the C/ash content increased. A greater amount of carbon available for the reaction improved the electrochemical performance, while a lower amount of ash limited the action of the inert fraction in the electrochemical reaction [53]. Coke and

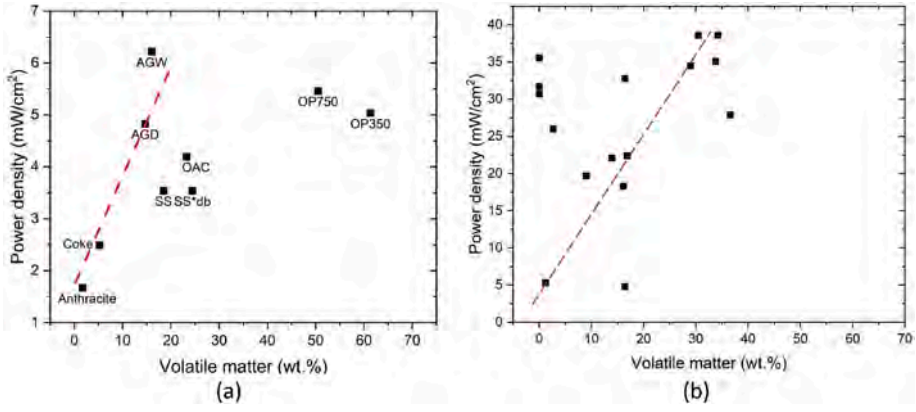

Fig. 12. Power density as function of volatile matter a) Data collected by the author; b) Data gathered from the literature review (Kacprzak et al. [24,29]).

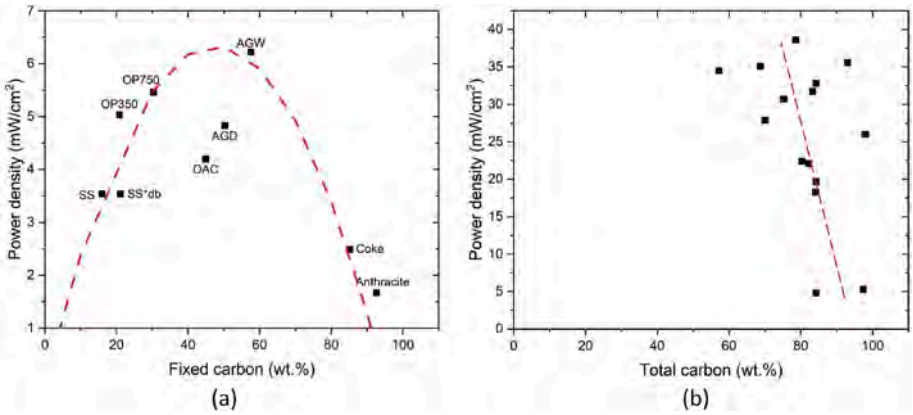

Fig. 13. Power density as function of fixed carbon a) Data collected by the author; b) Data gathered from the literature review (Kacprzak et al. [24,29]).

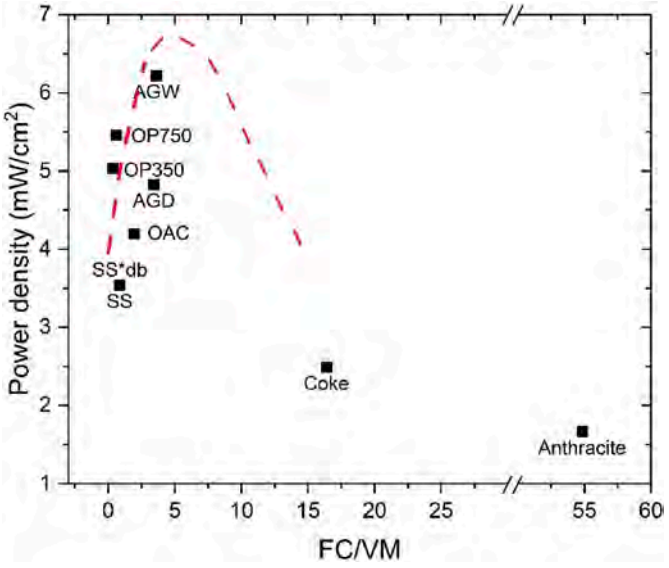

Fig. 14. Power density function of the ratio between fixed carbon and volatile matter.

Anthracite were outliers because the great amount of carbon limited the chemical activation overcoming any other influence of ash. On the contrary, the power density decreased when the VM/ash ratio increased (Fig. 16b) due to the progressive gasification of the VM that concentrated the fraction of ash in the tea-bag.

The amount of ash was an intrinsic limitation to electrochemical performance because it is an inert material that reduces the available carbon and causes side effects, such as blocking the pore structure and inhibiting the anode reaction [12]. Therefore, it was more reasonable to consider the chemistry of the ash than its quantity. This is because some of the ash could have a positive effect on the reaction.

The highest power densities were provided by OP350, OP750, AGW and AGD, most probably for the presence of sylvite (KCl) inside their ash. Wang et al. [76] demonstrated how using KCl as washing agent for biochar led to high oxidation activity and subsequent good DCFC performance. As said previously, KCl is used to enhance the carbon activation promoted by KOH, which in turns, results in better electrochemical performance. The high power density achieved with OP350 (5.04 mW cm^{-2}) was also caused by the elevated number of hydrogens contained in the hemicellulose ($(C_6H_{10}O_5)_n$ + $(C_5H_8O_4)_n$) (Fig. 3), which improved the electrochemical performances [12,13,27,77]. According to Kawase et al. [55], the elevated amount of water originated from the oxidation of H_2 positively affected the power generation. The chemical composition hence explained why OP350 and OP750 were outliers in Fig. 16b. In addition, the iron oxides in OAC e SS could overcame the limitations given by the high amount of ash, thanks to the catalytic effect of hematite (Fe_2O_3) and magnetite (Fe_3O_4) [37]. Compounds as quartz (SiO_2) instead limited the cell performances [12,27,37], due to the formation of a passivating membrane of M_2SiO_3 (where M is either K or Na) on the anode [65].

The resulting electrochemical performance of the cell was therefore influenced by three chemical factors: volatile matter, fixed carbon and ash content. These factors should be considered together, as well as how they interacted with each other. Kacprzak et al. [29] already highlighted the difficulty of defining exactly how the chemical composition of the fuel affected the electrochemical performance. They noted that carbon

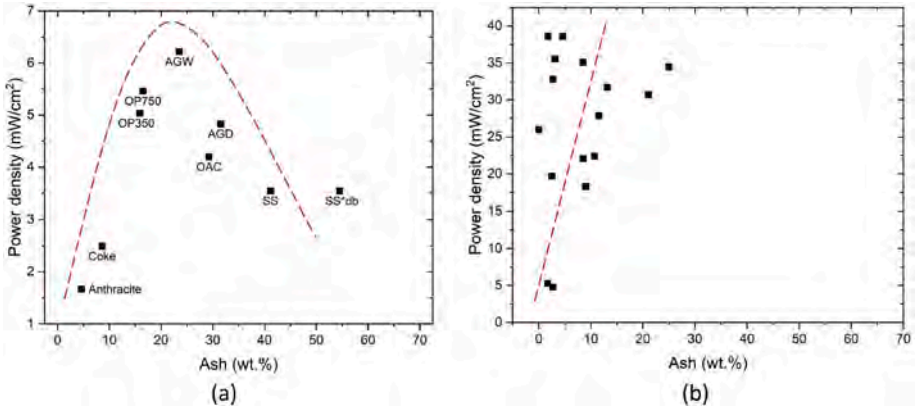

Fig. 15. a) Power density as function of ash content a) Data collected by the author; b) Data gathered from the literature review (Kacprzak et al. [24,29]).

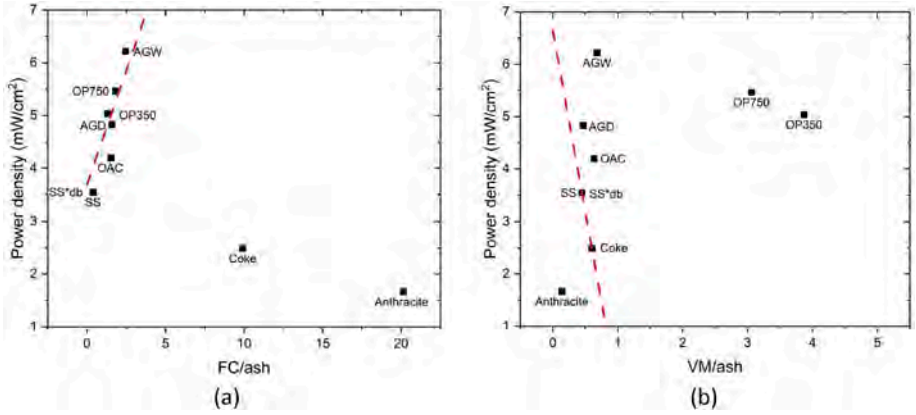

Fig. 16. Power density as function of the ratio between fixed carbon and ash; b) Power density as function of the ratio between volatile matter and ash.

content, ash and volatile matter affected the DCFC's operation in a non-linear way, and that their combination with other factors could influence the final result.

3.3.6. *Effect of aspect ratio, porosity and particles' dimension*

Another factor influencing the power density was the morphology of the fuel particles, particularly their aspect ratio (Fig. 17). The higher power density achieved with more elongated particles was probably due to their greater real surface area compared to circular particles, which only had one theoretical point of contact with the anode wall.

The difference in shape of fuel particle was considered as a limiting factor also by Kacprzak et al. [24], which attributed the not exact repeatability of the tests due to the random distribution of the particles with different geometry inside the anode container, as different contact between the anode wall and the particles affected the resulting performance of the fuel. However, a direct comparison between the electrochemical performance and the morphology of the fuel was difficult because the results were affected by the particles' geometric shape, dimensions, and porosity. For instance, the positive effect of an aspect ratio of 0.537 for OAC was offset by its high dimensions (380.34 ± 240.69 μm) and low porosity (24.38%), causing it to be an outlier in Fig. 17 (the standard deviation of ±0.266 however fits the trend; thus, the following discussion is based on the mean value reported in figure). The large standard deviation means a wide particle size distribution within the fuel, resulting in heterogeneous electrochemical behavior.

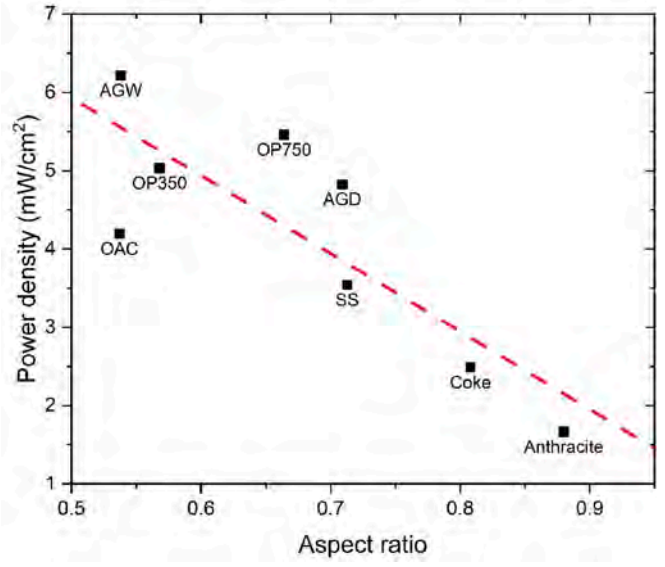

Fig. 17. Power density as function of the aspect ratio.

Fine particles typically provide higher performance due to their larger effective surface area and better contact with the anode, whereas coarser particles contribute less effectively to the electrochemical reaction and may limit the overall power output [14]. Consequently, the fuel's performance is determined by the balance between these fractions. The presence of a significant coarse particle fraction hence caused a practical limitation on the achievable electrochemical activity and leads to increased variability and instability in the measured properties. Conversely, the high interfacial surface given by the porosity increased the availability of sites for electrochemical reactions and, consequently, increased the electron flux generated in the DCFC [27].

This was explanatory of the higher power density of OP350 and OP750 (5.04 and 5.46 mW cm^{-2}) respect to Anthracite having the former two a porosity of 33.07 and 30.78% while the latter of 2.16%, which decreased the reactive area available and worsened cell performances [45]. On the other hand, this was not associable to the Coke behavior as, despite the high porosity (29.97%), the particles' dimension of 389.02 ± 144.89 μm limited its power density (2.49 mW cm^{-2}) due to limited surface area associated to larger particles [14]. This feature added to the high FC of coke well explained why its electrochemical performance was not satisfactory. As a further example, SS could be considered not optimized fuel from a morphological point of view, due to a mean dimension of 364.46 ± 139.5 μm and low porosity (12.83%). However, the unfavorable features were partially offset by the catalytic effect of SS ash, which produced a power density of 3.54 mW cm^{-2}.

3.3.7. *Effect of graphitization*

The power density was improved not only by disordered carbon in terms of elongated shape of the particles, but also by its poor crystallinity (Fig. 3) [45]. Less graphitized carbon is more reactive to oxidation than graphitized carbon, which has a low surface area and therefore limited reactive sites [27,36]. Indeed, the lowest power densities were observed in the two graphitic, carbon-rich materials (Anthracite and Coke).

3.3.8. *Intrinsic effect of the fuel cell*

The difficulties to define which were the ideal physicochemical properties of the fuel to reach the highest cell performances were already highlighted by Kacprzak et al. [29,53]. Although testing is necessary to ensure the performance of a fuel, this work helped to define how fuel properties affect the OCV and LSV results of a MH-DCFC more accurately. However, the operative conditions of the cell itself affected the results. For instance, the obtained power densities were of the same order of magnitude as that obtained by Kacprzak et al. [45] using a similar design and the same materials to build the cell, such as stainless steel in contact with a more noble material, like the Ni-alloy. However, the stainless steel is not the ideal material to build up this type of cell,

since its progressive corrosion negatively affected the cell performance [45]. In addition, carbon may be subject to property variation during power generation, resulting in a change in electrochemical performance compared to that predicted [36], but the characterization of the fuel after the test is difficult due to the contamination with the electrolyte. Another influencing factor was the duration of the test. Fig. 18 shows indeed a linear relationship between the time of OCV stabilization and power density. The LSV curves were collected just after the stabilization of the OCV, hence the carbon involved was only the one activated at that time. The power density of fuels which stabilize in short time was affected only by VM, resulting in low power density. Increasing the duration of the test, more carbon was probably activated, therefore resulting in higher power density.

3.4. Combined effects of fuel properties on MH-DCFC performance

The most promising carbon-rich materials were AGW (OCV: 1015 mV; power density: 6.22 mW cm^{-2}), OP750 (OCV: 1021 mV; power density: 5.46 mW cm^{-2}) and OP350 (OCV: 1060 mV; power density: 5.04 mW cm^{-2}). Despite their similar origin, no single common parameter could be identified as solely responsible for their better electrochemical performance. Rather, the results clearly indicate that MH-DCFC performance is governed by the combined and often non-linear interaction between morphological characteristics (such as porosity, particle size, and aspect ratio) and chemical properties (including volatile matter, fixed carbon, ash content, mineralogical composition, and wettability). The complexity of the chemical composition, together with the wide variability in particle morphology, prevents decoupling of individual effects, as each parameter contributes simultaneously to the electrochemical behavior. In particular, the best MH-DCFC performance was achieved using carbon-rich fuels characterized by a balanced FC/VM ratio of 1-2, a moderate ash content of 25-30 wt%, elongated and porous particles (aspect ratio of nearly 0.5 and porosity around 30%), and the presence of catalytically active mineral phases. Among the fuels tested, AGW clearly represents the optimal choice, as it combines both the favorable chemical composition and the desired morphological features, confirming that peak performance arises from the synergistic interaction of all factors rather than from a single parameter.

These observations are further supported by literature data [24,29], which report consistent trends for similar carbon-based fuels. In particular, the OCV values are generally comparable, while higher power density values are often achieved. Nevertheless, the relative performance ranking and overall trends remain unchanged, confirming that carbon fuel properties influence electrochemical performance in a consistent manner. Differences in absolute performance values are mainly attributable to fuel cell design optimization rather than to intrinsic fuel characteristics.

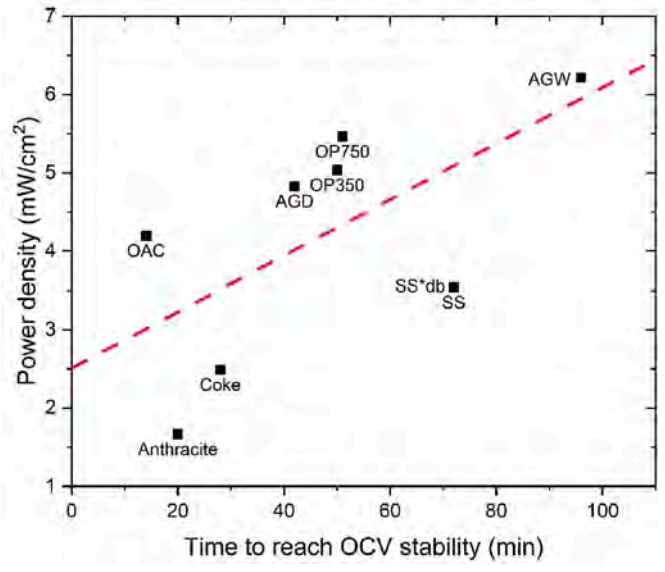

Fig. 18. Power density as function of the time to reach the stabilization of the OCV.

Within this multifactorial framework, so-called "outliers" should not be considered as anomalous or inconsistent data points, but rather as materials whose electrochemical behaviour cannot be explained by a single parameter taken in isolation. When individual correlations are considered (e.g., ash content, FC/VM ratio, particle size, or wettability), some fuels appear to deviate from the main trend. However, these deviations systematically disappear, or are significantly reduced, once additional physicochemical parameters are simultaneously taken into account. For instance, fuels such as OAC or SS had relatively high ash contents and non-optimal FC/VM ratios, which would typically be associated with poor electrochemical performance. Nevertheless, their measured OCV and power density are higher than expected because the chemical nature of the ash plays a dominant role. The presence of catalytically active phases, particularly iron oxides, enhances carbon gasification and electrochemical oxidation, partially offsetting the negative effects of ash accumulation and limited reactive carbon. Similarly, materials that appear as outliers in morphology-based correlations (e.g., aspect ratio for OAC or porosity for Coke) often align with alternative trends when particle size, mineralogical composition, or electrolyte-fuel interactions are considered. This indicates that deviations from simple linear correlations are not random, but instead reflect the complex nature of the system, where improvements in one property can compensate for deficiencies in another.

Although the absolute power densities obtained in this study are relatively low (maximum value of 6.22 mW cm^{-2}), the results demonstrate the practical potential of DCFCs to contribute to industrial energy production, particularly when fueled with carbon-containing residues. Consequently, the present results do not allow to exclude fuel with different properties to the ideal ones, but encourage the exploration of additional carbon-rich residues, such as active carbons recovered from quenching towers or other steelmaking by-products like blast furnace sludge, as potentially viable fuels for MH-DCFCs, even when their individual chemical composition might initially appear complex. Additionally, the working temperature of 450 °C allows the recovery of process heat and the valorization of top-gas, enhancing overall system efficiency. While, the modular nature of DCFCs allows multiple cells to be stacked or integrated, enabling a cumulative increase in energy output despite the limited performance of individual units. These findings provide a solid foundation for future improvements, including the use of Ni-alloy materials for both anode and cathode components, optimized cell geometries, and scale-up strategies, all of which are expected to significantly increase absolute power density. According to Dall'Osto et al. [25], DCFCs alone could satisfy the 10% of electrical demand of steelmaking industry. Their integration into processes such as steelmaking could hence supply a meaningful fraction of energy requirements, representing a viable and important step toward decarbonization and a sustainable green transition in industry.

4. Conclusion

In this work, 9 carbon-rich fuels (including 7 biochars and 2 fossil materials) were first physicochemical characterized and subsequently short-term tested in MH-DCFC. By correlating the physicochemical characteristics of the fuels to their electrochemical behavior, this study explained how the key fuel properties affect OCV and power density in MH-DCFCs operating at 450 °C. The main fundings can be summarised as follows.

- Chemical composition and reactivity: An optimal range for electrochemical performance was identified at a FC/VM ratio of 1-2. Volatile matter enhances short-term activation and increases both OCV and power density, but excessively high VM leads to rapid volatilization, fuel loss, and performance decay. FC is essential for sustaining carbon oxidation once VM is depleted. Overly graphitized or highly crystalline carbon, typical of fossil fuels, reduces reactivity and yields lower electrochemical performance.
- Ash role: Ash content negatively affects cell performance when exceeding 30 wt%. However, ash composition matters more than quantity because catalytic species such as Fe_2O_3, Fe_3O_4 and $CaCO_3$ significantly improve reactivity and compensate for high ash fractions.
- Morphological properties: elongated and porous structures enhance electrolyte-fuel contact and electron transfer, while large or highly spherical particles limit reactive surface area and slow activation.
- Fuel performances in MH-DCFCs are influenced by a combined effect of chemical composition, ash and morphological properties rather than by any single parameter alone.
- Operational limitations: electrochemical performance is also affected by MH-DCFC design, including stainless steel corrosion, activation times, and incomplete fuel conversion, highlighting the need for improved cell materials and optimized the cell parameters.

CRediT authorship contribution statement

Sara Scolari: Writing – review & editing, Writing – original draft, Visualization, Validation, Methodology, Investigation, Formal analysis, Data curation, Conceptualization. **Davide Mombelli:** Writing – review & editing, Validation, Methodology, Investigation, Formal analysis, Data curation, Conceptualization. **Gianluca Dall'Osto:** Writing – review & editing, Validation. **Carlo Mapelli:** Writing – review & editing, Validation, Supervision, Conceptualization.

Declaration of competing interest

The authors declare that they have no known competing financial interests or personal relationships that could have appeared to influence the work reported in this paper.

Acknowledgements

The Authors would like to acknowledge European Union - NextGenerationEU, under the National Recovery and Resilience Plan (PNRR), Mission 4, Component 2, Investment 1.1, PRIN PNRR 2022 project - JETCELL, CUP D53D23018060001, Prot. P20225LHPX. The Authors would like to acknowledge European Union - NextGenerationEU, M4C2 I1.1, PRIN 2022 project -"Low environmental impact fuels for metallurgical industries", CUP D53D23003860006, Prot. 2022P3PJXN. The Authors would like to acknowledge BioRECAST, this project has received funding by the European Commission from the Research Fund for Coal and Steel under grant agreement 101112601.

List of symbols

AGD	Agricultural digestate
AGW	Agricultural waste
AR	Aspect ratio
FC	Fixed carbon
LSV	Linear sweep voltammetry
OAC	Olive acquachar
OCV	Open circuit voltage
OP350	Olive pomace pyrolyzed at 350 °C
OP750	Olive pomace pyrolyzed at 750 °C
SS	Sewage sludge
VM	Volatile matter
WR	Wood residues

Appendix A. Supplementary data

Supplementary data to this article can be found online at https://doi.org/10.1016/j.biombioe.2026.109151.

Data availability

Data will be made available on request.

References

[1] https://ember-energy.org/app/uploads/2025/01/EER_2025_22012025.pdf. (Accessed 9 October 2025).
[2] H. Sethia, A. Priyam, Review on hydrogen fuel cells as an alternative fuel, Next Energy 9 (Oct. 2025) 100460, https://doi.org/10.1016/j.nxener.2025.100460.
[3] N. Radenahmad, et al., A review on biomass derived syngas for SOFC based combined heat and power application, Renew. Sustain. Energy Rev. 119 (Mar. 2020) 109560, https://doi.org/10.1016/j.rser.2019.109560.
[4] F.K. Kazeroonian, M.R. Rahimpour, Application of syngas in fuel cell, in: Advances in Synthesis Gas : Methods, Technologies and Applications, Elsevier, 2023, pp. 337–367, https://doi.org/10.1016/B978-0-323-91878-7.00021-6.
[5] N. Radenahmad, J. Taweekun, A. Afif, J.-Y. Park, J. Zaini, A.K. Azad, Syngas fuelled high performance solid oxide fuel cell, ECS Trans. 91 (1) (Jul. 2019) 1621–1629, https://doi.org/10.1149/09101.1621ecst.
[6] P. Costa, F. Pinto, R.N. André, P. Marques, Integration of gasification and solid oxide fuel cells (SOFCs) for combined heat and power (CHP), Processes 9 (2) (Jan. 2021) 254, https://doi.org/10.3390/pr9020254.
[7] N. Ozalp, et al., An overview of direct carbon fuel cells and their promising potential on coupling with solar thermochemical carbon production, Renew. Sustain. Energy Rev. 162 (Jul. 2022) 112427, https://doi.org/10.1016/j.rser.2022.112427.
[8] S. Giddey, S.P.S. Badwal, A. Kulkarni, C. Munnings, A comprehensive review of direct carbon fuel cell technology, Prog. Energy Combust. Sci. 38 (3) (Jun. 2012) 360–399, https://doi.org/10.1016/j.pecs.2012.01.003.
[9] L. Kouchachvili, P. Geddis, Q. Zhuang, Direct carbon fuel cell design for continuous operation, Int. J. Hydrogen Energy 46 (9) (Feb. 2021) 6792–6802, https://doi.org/10.1016/j.ijhydene.2020.11.179.
[10] K. Xu, et al., Investigation of the anode reactions in SO-DCFCs fueled by Sn–C mixture fuels, Proc. Combust. Inst. 36 (3) (2017) 4435–4442, https://doi.org/10.1016/j.proci.2016.06.171.
[11] S. Li, W. Pan, S. Wang, X. Meng, C. Jiang, J.T.S. Irvine, Electrochemical performance of different carbon fuels on a hybrid direct carbon fuel cell, Int. J. Hydrogen Energy 42 (25) (Jun. 2017) 16279–16287, https://doi.org/10.1016/j.ijhydene.2017.05.150.
[12] C. Jiang, J. Ma, A. Arenillas, A.D. Bonaccorso, J.T.S. Irvine, Comparative study of durability of hybrid direct carbon fuel cells with anthracite coal and bituminous coal, Int. J. Hydrogen Energy 41 (41) (Nov. 2016) 18797–18806, https://doi.org/10.1016/j.ijhydene.2016.04.047.
[13] A. Fuente-Cuesta, C. Jiang, A. Arenillas, J.T.S. Irvine, Role of coal characteristics in the electrochemical behaviour of hybrid direct carbon fuel cells, Energy Environ. Sci. 9 (9) (2016) 2868–2880, https://doi.org/10.1039/C6EE01461E.
[14] M. Ahsan, P. Fu, H. Guo, B. Wei, An investigation to enhance the performance of molten carbonate-direct coal/carbon fuel cells through improvements in anode layouts and the compositions of carbonate electrolyte, Appl. Therm. Eng. 243 (Apr. 2024) 122761, https://doi.org/10.1016/j.applthermaleng.2024.122761.
[15] M. Dudek, P. Tomczyk, R. Socha, M. Skrzypkiewicz, J. Jewulski, Biomass fuels for direct carbon fuel cell with solid oxide electrolyte, Int. J. Electrochem. Sci. 8 (3) (Mar. 2013) 3229–3253, https://doi.org/10.1016/S1452-3981(23)14386-0.
[16] K. Xu, et al., Evaluation of biomass and its thermal decomposition products as fuels for direct carbon fuel cells, Biomass Bioenergy 130 (Nov. 2019) 105359, https://doi.org/10.1016/j.biombioe.2019.105359.
[17] S. Li, et al., Mechanism of enhanced performance on a hybrid direct carbon fuel cell using sawdust biofuels, J. Power Sources 383 (Apr. 2018) 10–16, https://doi.org/10.1016/j.jpowsour.2018.02.040.
[18] A. Elleuch, K. Halouani, Y. Li, Investigation of chemical and electrochemical reactions mechanisms in a direct carbon fuel cell using olive wood charcoal as sustainable fuel, J. Power Sources 281 (May 2015) 350–361, https://doi.org/10.1016/j.jpowsour.2015.01.171.
[19] D. Pauluzzi, A. Martinis, SUSTAINABLE DECREASE OF CO2 EMISSIONS IN THE STEELMAKING INDUSTRY BY MEANS OF THE ENERGIRON DIRECT REDUCTION TECHNOLOGY, 2018.
[20] F.A. García, P. Campoy, Javier Mochón, I. Ruiz-Bustinza, L.F. Verdeja, R.M. Duarte, A new 'User-friendly' blast furnace advisory control System using a neural network temperature profile classifier, ISIJ Int. 50 (5) (2010) 730–737, https://doi.org/10.2355/isijinternational.50.730.
[21] N. Müller, G. Herz, E. Reichelt, M. Jahn, A. Michaelis, Assessment of fossil-free steelmaking based on direct reduction applying high-temperature electrolysis, Clean. Eng. Technol. 4 (Oct. 2021) 100158, https://doi.org/10.1016/j.clet.2021.100158.

[22] A. Salimbeni, G. Lombardi, A.M. Rizzo, D. Chiaramonti, Techno-Economic feasibility of integrating biomass slow pyrolysis in an EAF steelmaking site: a case study, Appl. Energy 339 (Jun. 2023) 120991, https://doi.org/10.1016/j.apenergy.2023.120991.
[23] L. Guo, J.M. Calo, E. DiCocco, E.J. Bain, Development of a low temperature, molten hydroxide direct carbon fuel cell, Energy & Fuels 27 (3) (Mar. 2013) 1712–1719, https://doi.org/10.1021/ef302100h.
[24] A. Kacprzak, R. Kobyłecki, R. Włodarczyk, Z. Bis, The effect of fuel type on the performance of a direct carbon fuel cell with molten alkaline electrolyte, J. Power Sources 255 (Jun. 2014) 179–186, https://doi.org/10.1016/j.jpowsour.2014.01.012.
[25] G. Dall'Osto, D. Mombelli, A. Pittalis, C. Mapelli, Biochar and other carbonaceous materials used in steelmaking: possibilities and synergies for power generation by direct carbon fuel cell, Biomass Bioenergy 177 (Oct. 2023) 106930, https://doi.org/10.1016/j.biombioe.2023.106930.
[26] A. Kacprzak, R. Kobyłecki, R. Włodarczyk, Z. Bis, Efficiency of non-optimized direct carbon fuel cell with molten alkaline electrolyte fueled by carbonized biomass, J. Power Sources 321 (Jul. 2016) 233–240, https://doi.org/10.1016/j.jpowsour.2016.04.132.
[27] N. Grioui, A. Elleuch, K. Halouani, Y. Li, Valorization of exhausted olive pomace for the production of a fuel for direct carbon fuel cell, C (Basel). 9 (1) (Feb. 2023) 22, https://doi.org/10.3390/c9010022.
[28] N. Kaklidis, et al., Effect of carbon type on the performance of a direct or hybrid carbon solid oxide fuel cell, RSC Adv. 4 (36) (2014) 18792–18800, https://doi.org/10.1039/C4RA01022A.
[29] A. Kacprzak, R. Kobyłecki, Zbigniew Bis, The effect of coal thermal pretreatment on the electrochemical performance of molten hydroxide direct carbon fuel cell (MH-DCFC), Journal of Power Technologies 97 (5) (2018) 382–387.
[30] G. Dall'Osto, S. Scolari, D. Mombelli, C. Mapelli, Survey on the valorization of wood and agribusiness wastes for their application as fossil carbon substitutes in metallurgical processes, Biomass Convers. Biorefin. (Mar. 2025), https://doi.org/10.1007/s13399-025-06707-1.
[31] C.P. Ezeakacha, A. Rabbani, S. Salehi, A. Ghalambor, Integrated image processing and computational techniques to characterize Formation damage, in: SPE International Conference and Exhibition on Formation Damage Control, SPE, Feb. 2018, https://doi.org/10.2118/189509-MS.
[32] A. Rabbani, S. Salehi, Dynamic modeling of the formation damage and mud cake deposition using filtration theories coupled with SEM image processing, J. Nat. Gas Sci. Eng. 42 (Jun. 2017) 157–168, https://doi.org/10.1016/j.jngse.2017.02.047.
[33] L. Zhao, Y. Li, M. Yu, Y. Peng, F. Ran, Electrolyte-Wettability issues and challenges of electrode materials in electrochemical energy storage, energy conversion, and beyond, Adv. Sci. 10 (17) (Jun. 2023), https://doi.org/10.1002/advs.202300283.
[34] H.W. Otto, R.P. Seward, Phase equilibria in the potassium hydroxide-sodium hydroxide System, J. Chem. Eng. Data 9 (4) (Oct. 1964) 507–508, https://doi.org/10.1021/je60023a009.
[35] J.A. Allen, J. White, M. Glenn, S.W. Donne, Molten carbonate composition effects on carbon electro-oxidation at a solid anode interface, J. Electrochem. Soc. 162 (1) (Nov. 2015) F76–F83, https://doi.org/10.1149/2.0321501jes.
[36] N.J. Cherepy, R. Krueger, K.J. Fiet, A.F. Jankowski, J.F. Cooper, Direct conversion of carbon fuels in a molten carbonate fuel cell, J. Electrochem. Soc. 152 (1) (2005) A80, https://doi.org/10.1149/1.1836129.
[37] X. Li, Z. Zhu, R. De Marco, J. Bradley, A. Dicks, Evaluation of raw coals as fuels for direct carbon fuel cells, J. Power Sources 195 (13) (Jul. 2010) 4051–4058, https://doi.org/10.1016/j.jpowsour.2010.01.048.
[38] Z. Kovačević, S. Bischof, N. Bilandžija, T. Krička, Conversion of Waste agricultural biomass from straw into useful Bioproducts—Wheat fibers and biofuels, Sustainability 16 (11) (Jun. 2024) 4739, https://doi.org/10.3390/su16114739.
[39] I.G. Edeh, O. Masek, F. Fusseis, 4D structural changes and pore network model of biomass during pyrolysis, Sci. Rep. 13 (1) (Dec. 2023) 22863, https://doi.org/10.1038/s41598-023-49919-z.
[40] M. Zou, et al., Corrected Pore size distribution and structure parameters in anthracite coal from Mercury intrusion and nitrogen adsorption, Energy & Fuels 39 (45) (Nov. 2025) 21909–21917, https://doi.org/10.1021/acs.energyfuels.5c04791.
[41] https://www.drawellanalytical.com/xrd-for-amorphous-and-crystalline-polymers-what-to-look-for/. (Accessed 8 October 2025).
[42] J. Wang, et al., The role of residual char on ash flow behavior, Part 1: the effect of graphitization degree of residual char on ash fusibility, Fuel 234 (Dec. 2018) 1173–1180, https://doi.org/10.1016/j.fuel.2018.08.011.
[43] Y. Wu, Z. Zhao, H. Li, F. He, Low temperature pyrolysis characteristics of major components of biomass, J. Fuel Chem. Technol. 37 (4) (Aug. 2009) 427–432, https://doi.org/10.1016/S1872-5813(10)60002-3.
[44] L. Gao, J.R. Selman, P. Nash, Materials and wetting issues in molten carbonate fuel cell technology: a review, J. Mater. Sci. 58 (41) (Nov. 2023) 15936–15972, https://doi.org/10.1007/s10853-023-08958-7.
[45] A. Kacprzak, R. Włodarczyk, Materials selection and construction development for ensuring the availability and durability of the molten hydroxide electrolyte direct carbon fuel cell (MH-MCFC), Materials 13 (20) (Oct. 2020) 4659, https://doi.org/10.3390/ma13204659.
[46] S.Y. Ahn, et al., Utilization of wood biomass char in a direct carbon fuel cell (DCFC) system, Appl. Energy 105 (May 2013) 207–216, https://doi.org/10.1016/j.apenergy.2013.01.023.
[47] S. He, S.P. Jiang, Electrode/electrolyte interface and interface reactions of solid oxide cells: recent development and advances, Prog. Nat. Sci. Mater. Int. 31 (3) (Jun. 2021) 341–372, https://doi.org/10.1016/j.pnsc.2021.03.002.
[48] J.F. Cooper, R. Selman, Electrochemical oxidation of carbon for electric power generation: a review, ECS Trans. 19 (14) (Oct. 2009) 15–25, https://doi.org/10.1149/1.3220176.
[49] V. Hoffmann, et al., Conductive carbon materials from the hydrothermal carbonization of vineyard residues for the application in electrochemical double-layer capacitors (EDLCs) and direct carbon fuel cells (DCFCs), Materials 12 (10) (May 2019) 1703, https://doi.org/10.3390/ma12101703.
[50] https://www.malvernpanalytical.com/en/learn/knowledge-center/application-notes/an170103batteryslurryparticlesizeshape. (Accessed 13 November 2025).
[51] K. Araújo Soares, J.A. Schembek Silva, X. Wang, A. Valente Bueno, F. Leite Lobo, Tools for enhancing extracellular electron transfer in bioelectrochemical systems: a review, Fermentation 11 (7) (Jun. 2025) 381, https://doi.org/10.3390/fermentation11070381.
[52] W.H.A. Peelen, J.H.W. de Wit, Carbon A MAJOR ENERGY CARRIER FOR THE FUTURE, in: European Research Conference on Molten Salts, June 27th – July 3rd, Poquerolles, France, 1998.
[53] A. Kacprzak, R. Włodarczyk, Utilization of organic waste in a direct carbon fuel cell for sustainable electricity generation, Energies 16 (21) (Oct. 2023) 7359, https://doi.org/10.3390/en16217359.
[54] A. Modjtahedi, N. Hedayat, S.S.C. Chuang, The direct carbon solid oxide fuel cell with H2 and H2O feeds, Solid State Ion. 268 (Dec. 2014) 15–22, https://doi.org/10.1016/j.ssi.2014.09.014.
[55] M. Kawase, A. Ido, Performance and sulfur tolerance of direct biomass fuel cells, J. Power Sources 642 (Jun. 2025) 236880, https://doi.org/10.1016/j.jpowsour.2025.236880.
[56] C.-G. Lee, Y.-J. Kim, T.-K. Kim, S.-W. Lee, Characteristics of solid fuel oxidation in a molten carbonate fuel cell, Journal of Electrochemical Science and Technology 7 (2) (Jun. 2016) 91–96, https://doi.org/10.5229/JECST.2016.7.2.91.
[57] M. Eskezia, Electrochemical power generation from carbon in fuel cell with molten hydroxide electrolyte, International Journal of Advanced Research in Chemical Science 7 (6) (2020), https://doi.org/10.20431/2349-0403.0706003.
[58] S.L. Jain, Y. Nabae, B.J. Lakeman, K.D. Pointon, J.T.S. Irvine, Solid state electrochemistry of direct carbon/air fuel cells, Solid State Ion 179 (27–32) (Sep. 2008) 1417–1421, https://doi.org/10.1016/j.ssi.2008.01.078.
[59] K. Crombie, O. Mašek, Pyrolysis biochar systems, balance between bioenergy and carbon sequestration, GCB Bioenergy 7 (2) (Mar. 2015) 349–361, https://doi.org/10.1111/gcbb.12137.
[60] M. Simoni, et al., Decarbonisation of calcium carbonate in sodium hydroxide solutions under ambient conditions: effect of residence time and mixing rates, Phys. Chem. Chem. Phys. 24 (26) (2022) 16125–16138, https://doi.org/10.1039/D2CP01412B.
[61] M. Simoni, et al., Synthesis of $Ca(OH)_2$ and Na_2CO_3 through anion exchange between $CaCO_3$ and NaOH: effect of reaction temperature, RSC Adv. 12 (49) (2022) 32070–32081, https://doi.org/10.1039/D2RA05827H.
[62] M. Skrzypkiewicz, I. Lubarska-Radziejewska, J. Jewulski, The effect of Fe2O3 catalyst on direct carbon fuel cell performance, Int. J. Hydrogen Energy 40 (38) (Oct. 2015) 13090–13098, https://doi.org/10.1016/j.ijhydene.2015.07.132.
[63] W. Cai, Q. Zhou, Y. Xie, J. Liu, A facile method of preparing Fe-loaded activated carbon fuel for direct carbon solid oxide fuel cells, Fuel 159 (Nov. 2015) 887–893, https://doi.org/10.1016/j.fuel.2015.07.030.
[64] I. Barin, Thermochemical Data of Pure Substances, third ed., 1995. Weinheim (Germany).
[65] C. Cui, et al., Review of molten carbonate-based direct carbon fuel cells, Mater. Renew. Sustain. Energy 10 (2) (Jul. 2021) 12, https://doi.org/10.1007/s40243-021-00197-7.
[66] S. Zecevic, E.M. Patton, P. Parhami, Direct electrochemical power generation from carbon IN fuel cells with molten hydroxide electrolyte, Chem. Eng. Commun. 192 (12) (Dec. 2005) 1655–1670, https://doi.org/10.1080/009864490896241.
[67] Q. Liu, Y. Tian, C. Xia, L.T. Thompson, B. Liang, Y. Li, Modeling and simulation of a single direct carbon fuel cell, J. Power Sources 185 (2) (Dec. 2008) 1022–1029, https://doi.org/10.1016/j.jpowsour.2008.08.100.
[68] E. Gürbüz, E. Grépin, A. Ringuedé, V. Lair, M. Cassir, Significance of molten hydroxides with or without molten carbonates in high-temperature electrochemical devices, Front. Energy Res. 9 (Apr. 2021), https://doi.org/10.3389/fenrg.2021.666165.
[69] Y. Han, H. Zhang, Z. Hu, S. Hou, Thermodynamic performance evaluation on a molten hydroxide direct carbon fuel cell with asymmetric anode and cathode, Int. J. Electrochem. Sci. 15 (9) (Sep. 2020) 8849–8872, https://doi.org/10.20964/2020.09.64.
[70] L. Xing, J. Hao, X. Li, Y. Zhang, Z. Hu, Y. Gao, Polarization modeling and performance optimization of a molten sodium hydroxide direct carbon fuel cell (MHDCFC), J. Power Sources 363 (Sep. 2017) 428–441, https://doi.org/10.1016/j.jpowsour.2017.07.113.
[71] I.C. Gómez, O.F. Cruz, J. Silvestre-Albero, C.R. Rambo, M.M. Escandell, Role of KCl in activation mechanisms of KOH-chemically activated high surface area carbons, J. CO2 Util. 66 (Dec. 2022) 102258, https://doi.org/10.1016/j.jcou.2022.102258.
[72] M. Glenn, B. Mathan, M.M. Islam, Y. Beyad, J.A. Allen, S.W. Donne, Gas atmosphere effects over the anode compartment of a tubular direct carbon fuel cell module, Energy & Fuels 33 (8) (Aug. 2019) 7901–7907, https://doi.org/10.1021/acs.energyfuels.9b01727.
[73] A. Kacprzak, R. Kobylecki, Z. Bis, Influence of temperature and composition of NaOH–KOH and NaOH–LiOH electrolytes on the performance of a direct carbon fuel cell, J. Power Sources 239 (Oct. 2013) 409–414, https://doi.org/10.1016/j.jpowsour.2013.03.159.

[74] C. Jiang, J. Ma, A. Arenillas, J.T.S. Irvine, Hybrid direct carbon fuel cells with different types of mineral coal, ECS Trans. 57 (1) (Oct. 2013) 3013–3021, https://doi.org/10.1149/05701.3013ecst.

[75] A.C. Chien, A. Arenillas, C. Jiang, J.T.S. Irvine, Performance of direct carbon fuel cells operated on coal and effect of operation mode, J. Electrochem. Soc. 161 (5) (Mar. 2014) F588–F593, https://doi.org/10.1149/2.025405jes.

[76] J. Wang, et al., A high-performance direct carbon fuel cell with Reed rod biochar as fuel, J. Electrochem. Soc. 166 (4) (Feb. 2019) F175–F179, https://doi.org/10.1149/2.0321904jes.

[77] K. Xu, C. Chen, H. Liu, Y. Tian, X. Li, H. Yao, Effect of coal based pyrolysis gases on the performance of solid oxide direct carbon fuel cells, Int. J. Hydrogen Energy 39 (31) (Oct. 2014) 17845–17851, https://doi.org/10.1016/j.ijhydene.2014.08.133.